THE EFFECT OF HEATING ON

BOUNDARY LAYER TRANSITION

FOR

LIQUID FLOW IN A TUBE

by

ROBERT SIEGEL

Research Assistant in Mechanical Engineering

and

ASCHER H. SHAPIRO

Professor of Mechanical Engineering

June, 1953

DEPARTMENT OF MECHANICAL ENGINEERING
MASSACHUSETTS INSTITUTE OF TECHNOLOGY
CAMBRIDGE, MASSACHUSETTS

CONTENTS

page

LIST OF TABLES

page

I. SUMMARY

An experimental investigation has been carried out to determine the effect of heating on boundary layer transition in a liquid. For this purpose water was circulated through a steam-heated smooth brass tube over a range of diameter Reynolds numbers from 30,000 to 140,000. With the disturbance level present in the system it was possible to produce adiabatic length Reynolds numbers of transition up to 850,000. The location of transition was determined from measurements of local apparent friction factor along the tube, and also by the use of a boundary layer probe which detected the change in velocity profile at the onset of transition. Heating was found to have no significant effect on the position of transition, and resulted in a slight decrease of free-stream length Reynolds number of transition, while the mean boundary layer Reynolds number of transition was slightly increased. Small roughnesses on the boundary walls were found to have a very pronounced effect on the location of transition.

The results indicate that for an ordinary water flow system, the use of heating could not be expected to appreciably cause stabilization of the laminar boundary layer.

An expression for local apparent friction factor in the laminar entry of a tube has been developed by the use of an approximate boundary layer computation method. The relation derived applies within a range where Re_x/Re_D^2 is less than 10^{-3}.

A second solution for apparent friction factor, which applies throughout the whole laminar entry region of a tube, has been derived by substituting an approximate velocity profile shape into the continuity and momentum equations. The velocity profile chosen approached flat plate behavior near the tube entrance, and gradually changed toward a parabolic shape as the flow developed. Graphical integration was used to obtain the final results in tabular form.

II. INTRODUCTION

Brief Introduction to Mathematical Stability Theory

The current concept of the process governing the transition of a boundary layer from laminar to turbulent motion is based on stability considerations. At a certain critical value of the Reynolds number, the flow becomes unstable for small disturbances, which then amplify until the motion becomes turbulent. The point at which the critical Reynolds number is attained is termed the instability point, while the point at which the boundary layer begins to deviate from laminar motion is called the transition point. Between the two lies the zone in which small disturbances undergo amplification. Since the mathematical investigations deal with the criteria for the growth of a small disturbance in the stream, it should be noted that they predict the location of the instability point, and not that of the transition point.

The general approach to the problem has been to superimpose a small disturbance motion upon the differential equations governing the basic flow. Only first order terms of the small perturbation velocity are retained, and the amplitude of the disturbance motion is investigated as a function of time. These calculations, carried out by Tollmien[22,23]*, Schlichting[17], and others, have shown that the critical Reynolds number is a function of the frequency of the disturbance, and also of the shape of the velocity profile. If the behavior for profiles with and without inflection points is compared, it is found, in general, that those having inflections are unstable over a wider range of frequencies than those without inflections. Moreover, the value of the critical Reynolds number, below which the flow is completely stable for all disturbances, is lower in the former case. Since the shape of the velocity profile can be altered by pressure gradients in the direction of motion, or by temperature distribution across the

---

* Superscripts in parenthesis refer to reference numbers in the bibliography.

boundary layer, these factors have an effect on the predicted stability of the flow.

Using the extension of the theory for the case of a compressible fluid[9,11], numerical calculations have been carried out for gases flowing past a flat plate. The calculations predict, in the case of air, an increase in stability when the plate is cooled and a decrease when the plate is heated. This comes about because an inflection point tends to be developed in the velocity profile for the case of a gas flowing over a hot plate. Since the rate of change of viscosity with temperature in a liquid is negative, whereas in a gas it is positive, it might be expected by analogy that the heating of a plate with liquid flowing over it would tend to increase laminar stability, although this case has not been adequately treated at present.

Summary of Experimental Work

Adiabatic experiments carried out by Schubauer and Skramstad[19] have fully substantiated the theoretical dependence of stability on both the frequency of the disturbance, and the external pressure gradient. Experiments by Liepmann and Fila[10] have shown that the boundary layer velocity profile for air passing over a heated flat plate develops an inflection, and that the transition point is caused to move upstream as heat is applied. Experiments by Scherrer[15] for cooling an air stream flowing externally over a cone at Mach number greater than unity, have shown a small increase in the transition Reynolds number, but the increases were much less than that predicted by theory. In the case of internal flows, recent investigations by Kline and Shapiro[6] for cooling air flowing within a smooth tube have shown no appreciable effect on the transition point even when the wall temperature was reduced over 200°F below the stream air temperature. These results clearly demonstrate that more experimental work on the effect of temperature gradients on stability is needed before a full understanding can be obtained.

Nature of the Present Investigation

In the present work, water was circulated through a tube with heated walls to determine whether transition could be delayed by this means. If successful, this technique would have application in reducing the surface drag on under-sea projectiles, on submarines, and in the inlets of hydraulic machines. Since the mathematical theory predicts only the instability point for motion with vanishingly small disturbances, it was necessary to resort to experiment to determine whether the theoretical trends for stability apply also to the behavior of the transition point in a fluid stream with a small but finite disturbance level.

III. DESCRIPTION OF THE TEST APPARATUS

Flow System

A schematic representation of the water recirculating system used for this investigation is shown in Figure 1. Water drawn from the city main was contained within a five hundred gallon storage tank and circulated through the test equipment by means of a five horsepower centrifugal pump. A by-pass back into the tank was provided at the pump discharge for the purpose of flow regulation. The piping was arranged so that the entire flow could be diverted at low velocity through a filter to be carefully cleaned before introduction into the test section. A standard orifice meter was located in the main line and mounted according to ASME specifications[25].

Stilling Chamber

From the main line the flow passed through a conical diffuser fabricated of galvanized sheet metal. The diffuser helped to prevent the formation of large scale turbulence during the transition from the three inch pipe line to the ten inch diameter stilling chamber. Following the diffuser the water entered a ten inch pipe tightly packed with approximately two thousand thin walled, extruded aluminum tubes having a length diameter ratio of forty (Figure 2). This honeycomb was sized to insure laminar flow in and between the tubes for all flow rates that were anticipated during the tests, and was employed to remove any swirling motion from the fluid.

A stilling chamber containing a series of fifteen turbulence damping screens was located after the honeycomb. The chamber design was such that it should theoretically provide about a two hundred fold reduction of the entering turbulence intensity. The screens chosen, according to the data of references 2, 3, 4, and 20, were 34 mesh and had a wire diameter of 0.0065 inches. Each was tightly stretched and soldered to an interlocking annular ring as shown in Figures 2 and 3. The screens were spaced two inches apart so that any low scale turbulence generated by a screen would be damped before the next screen was reached. The combination of chamber

size, wire diameter, and mesh number, was chosen such that a critical Reynolds number would not be exceeded, that is, vortices would not be shed from the screen wires for the range of flow rates used. Before entrance into the test section, a further reduction in turbulence was obtained due to the large reduction in cross-sectional area when the stream was contracted from the ten inch diameter chamber to the two inch diameter test section.

Contraction Nozzles

Following the stilling chamber the flow passed through a double contraction nozzle, going first from 10 to 4 1/2 inches and then from 4 1/2 to 2 inches in diameter. Each contraction was carefully machined to a double cubic contour according to the data of Rouse and Hassan[14], so as to avoid any unfavorable pressure gradients which might induce boundary layer separation. The finish machining was completed with the two contractions clamped together so that a smooth joint would be assured, and the whole interior was buffed to a high luster.

The wall of the second contraction was hollow (Figure 3), and cooling water could be circulated through it during the heated runs in order that it might be maintained at the same temperature as the water entering the test section. This was necessary because the contraction could not be effectively thermally isolated from the steam jacket used to heat the test pipe. Without cooling of the contraction walls, there would have resulted an undesirable thermal boundary layer formation in the stream before reaching the test section.

Design of the Test Section

The test section was constructed from a 2 inch internal diameter drawn, seamless brass tube 96 inches long and with a 0.125 inch wall thickness. At the entrance of the section a boundary layer suction slot was provided, through which up to 10 percent of the flow could be removed. The slot was designed according to specifications obtained from reference 12, and the configuration used is shown in Figure 4. The water removed passed from the

annular collection ring surrounding the slot, through eight copper tubes of equal length, and thence through the end-plate of the steam jacket into a collection header. The boundary layer flow was metered by a standard flange-tap orifice plate, and was returned to the main storage tank through an appropriate piping system and control valve.

The test pipe was provided with 18 wall static pressure taps, each having a diameter of 0.020 inches (Figure 4). These were spaced at distances in proportion to their distance from the boundary suction lip, except for the first few taps which were uniformly spaced 2 inches apart (see Table I). To prevent the build up of a disturbance from one tap to the next, the taps were successively spaced from one another at a helix angle of 110 degrees, so that no two taps were in line with the axial direction. The taps were carefully machined by alternate drilling and lapping operations to make them as uniform and square as possible, and to eliminate burrs at the inside edges. After the final drilling operation the whole tube was lapped and given a high polish on the inside.

Six thermocouples were mounted at intervals in tangential slots 1/16 inch deep, spaced on alternate sides of the test pipe (see Table II). The thermocouples were placed in the slots, and the slots filled with solder which was filed down flush with the outer tube wall.

The whole test section was enclosed within a steam jacket made of standard eight inch pipe. The jacket was provided with steam at 3 psi gage. All of the pressure tap and thermocouple connections were brought out through the steam jacket end-plate. The exit end of the test section was fixed to the steam jacket through a movable O-ring seal. This was done to prevent thermal stresses arising from the unequal expansion of the jacket and test pipe.

All of the return outlets in the storage tank were extended below the water surface to prevent splashing and subsequent entrainment of air bubbles by the water. In addition, each outlet was covered with two burlap bags,

the purpose being to disperse the water jets and to prevent the latter from inducing wave motions in the tank which would be transmitted back into the system as pressure fluctuations.

Instrumentation

Manometer System

In order to facilitate taking eighteen static pressure readings along the test section, two eighteen tube manometers were constructed so that all readings could be obtained at one time. One manometer was in a vertical position, and was used when the pressure differences between successive taps were comparatively large. For low flow rates, when the pressure differences were small, an inclined manometer was used. This was positioned to give the readings an amplification of five. Both manometers were provided with vents at their bases so that all air could be removed from the connecting lines.

Thermocouples

Thermocouples were used to measure the entrance and exit water temperatures of the test section, the temperature of the tube wall at six positions along its length, and the wall temperature of the small contraction nozzle. All of the thermocouples were made from the same spool of copper-constantan duplex wire and had welded junctions. The leads were brought into an isothermal zone box and were then connected through a selector switch to a standard laboratory potentiometer. A thermometer was suspended in the storage tank as a check on the average water temperature.

Orifice Meters

Standard ASME flange-tap orifice plates were used to measure the flow at pump discharge, and the quantity of water removed through the boundary layer suction slot. The flow in the test section was obtained as the difference between these two values. Both orifice unions were connected to vertical U-tube mercury manometers, and by the use of vents the connecting lines were kept filled with water.

Boundary Layer Probe

A boundary layer probe, constructed as shown in Figure 5, served as a second means of locating the transition point. The probe measured the static pressure on the axis of the tube, and the total pressure in the boundary layer at a fixed distance from the tube wall and in the same longitudinal plane as the static pressure. The probe was inserted through an O-ring seal at the exit end of the test pipe, and was calibrated in inches so that it could be positioned at any desired place along the tube.

IV. TEST PROCEDURE

At the beginning of the day in which the apparatus was being used, the storage tank was freshly filled from the city water mains, and then, by closing appropriate valves, the entire flow was diverted through the filter at low velocity and circulated back into the tank. This was continued for almost an hour to assure that essentially all of the water had passed through the filter and was as clean as possible. The main valves were then opened and a large flow allowed to circulate through the apparatus thus helping to expel any air which might be entrapped. In addition vents were opened to remove air trapped in the upper region of the honeycomb and stilling chamber. Steam was admitted to the jacket to heat the water to room temperature so that the temperature would remain substantially constant during the adiabatic runs. After the water had reached the proper condition the steam was shut off and the apparatus allowed to cool while the manometer lines were carefully purged of entrapped air. The main flow and boundary layer suction rates were then adjusted to the desired values for the experiment.

Runs Using Wall Static Pressure Taps

The first group of runs was taken using the pressure readings of the wall static pressure taps as the means of determining the transition point. At low flow rates the readings were taken from the inclined manometer, while at higher flow rates when the pressure differences between successive taps were larger, the vertical manometer was used. Immediately after taking an adiabatic run, the steam was turned on without making any changes in the valve settings. Cooling water was admitted to the storage tank (which was maintained at a constant level by an overflow pipe) to prevent the system temperature from rising as the result of heat added through the walls of the test section. It was found that some control over the size of the temperature difference across the wall could be obtained by the amount of venting

of the steam jacket. The more thoroughly the air was vented from the jacket the higher the temperature difference could be made, up to about 100°F, which was the upper limit for the low pressure steam employed. If high temperature differences were used it was found that non-condensible gases would come out of solution with the water, and air bubbles would collect in the manometer lines, thereby resulting in erroneous readings. When the wall pressure taps were used as a measuring means, the temperature differences were therefore kept small.

During the heated runs, cooling water was circulated through the jacket of the small contraction and regulated so that the contraction wall temperature was within a few degrees of the entering water temperature. In general a warming up period of at least an hour was necessary during the heated runs to achieve thermal equilibrium. During this period thermocouple readings were taken to aid in the regulation of the cooling water flow.

Runs Using the Boundary Layer Probe

For the runs using the boundary layer probe it was not necessary to vent the manometer lines, thus making it possible to reduce the starting time of the equipment. The connections of the probe to the inclined manometer were opened, the connections to the static wall taps were closed, and the lines running from the probe were thoroughly purged of air. The first reading was usually taken one inch downstream from the boundary layer suction slot, and successive readings were obtained at various intervals along the pipe by sliding the probe down the tube.

For a particular main stream flow, runs were made with various rates of boundary layer suction to determine whether or not the location of the transition point was sensitive to the suction rate. The runs with heat applied were then taken within a range where transition was insensitive to the suction rate, so that any change observed could not be attributed to slight differences in suction rate between the adiabatic runs and the

heated runs. Since, in the case of the boundary layer probe, all of the connecting lines ran down the interior of the test pipe and were therefore kept cool by the water flow, the difficulty of non-condensible gases collecting in the lines was not present and higher temperature differentials could be applied.

At the end of the running period the apparatus was completely drained to help minimize corrosion or electrolytic action between dissimilar metals within the system.

V. EXPERIMENTAL RESULTS

Methods Used to Determine the Location of Transition
Static Pressure Taps

When a fluid flows through a pipe entry, a laminar boundary layer grows which eventually enters a transition zone and becomes turbulent. The growth of the boundary layer is accompanied by momentum changes caused by altera- tions in the velocity profile as the flow pattern develops. Thus the difference in static pressure between two points along the pipe is a measure not only of the wall friction drop, but also includes the change due to momentum effects. The entire static pressure change between two points is expressed conveniently in dimensionless form as a local apparent friction factor, defined as follows:

$$4f_{APP} \equiv \frac{dp/d(x/D)}{\frac{1}{2}\rho v^2}$$

In the laminar zone the local apparent friction factor varies inversely as the one-half power of the length Reynolds number, and thus decreases along the length of the pipe. During transition the friction factor rises quite rapidly (it may drop at first under some circumstances) as the boundary layer thickens, and then begins to decrease slowly after the turbulent layer has formed. By considering a plot of $4f_{APP}$ vs. Re_x on logarithmic coordinates, the transition point can be determined where the curve begins to deviate from its original slope of negative one-half.

Boundary Layer Probe

The boundary layer probe was constructed to measure the static pressure along the axis of the tube in the core of the flow, as well as the total pressure in the boundary layer at a fixed distance from the wall. The difference between the two readings obtained is a direct indication of the local velocity at a fixed distance from the wall. Owing to the severe change in shape of the velocity profile at transition, this technique

provided a convenient means for locating the transition point.

As the boundary layer thickness increases along the tube in the laminar zone, the probe, located at increasing axial lengths but at a constant distance from the wall, becomes positioned proportionately deeper within the layer. Thus it is placed in a region of lower velocity, and a lower dynamic pressure is recorded as the difference between total and static pressure readings. In the laminar region, the curves of velocity pressure versus length Reynolds number have a negative slope similar to the local friction factor curves previously discussed. To further demonstrate this an approximate velocity profile for laminar flow over a flat plate was selected from reference 18, and calculations performed as indicated in Appendix B. This resulted in the illustrative curve shown in Figure 6. The calculated curve for the laminar zone shows the general trend of negative slope and agrees fairly well with the shape obtained experimentally in this region.

When the boundary layer becomes turbulent the resulting change in the shape of the velocity profile is reflected as an increase in the velocity pressure determined by the probe. The transition point is thus located as a well defined minimum on the curve of velocity pressure versus length Reynolds number.

Since the boundary layer probe was moved along the tube to obtain readings at various points, all of the readings were taken by the same instrument. Thus any small errors inherent in the instrument, (e.g., owing to irregularities in the pressure tap openings), remained substantially constant for all readings and did not cause any scatter of the data around the curves. Since the velocities used were fairly sizeable, the velocity pressure readings obtained were much larger than those due to friction drop. This allowed a wider margin of experimental reading error without causing noticeable scatter of the data. For these reasons the results obtained with the boundary layer probe produced, in general, better

experimental curves than the wall pressure tap method.

One question which immediately arises is whether the disturbance of the boundary layer probe in the test section may be transmitted upstream and possibly cause transition to occur earlier than if the probe were not present. To study this effect a run was made in which transition was determined by both methods, the wall static pressure readings being taken after the probe had been withdrawn beyond the end of the test section. The two curves, shown in Figures 7 and 8, both indicate transition at the same length Reynolds number of about 4.7×10^5. This demonstrates that the introduction of the probe did not significantly affect the position of the transition point.

Graphical Presentation of the Data

Either the local apparent friction factor or the velocity pressure in the boundary layer has been plotted against the length Reynolds number on logarithmic coordinates. The value of the average friction factor measured between two taps has to be plotted at a length Reynolds number corresponding to some mean value of x between the two points. In the laminar zone, as shown in reference 6, the appropriate mean value is the average of the arithmetic and geometric means of the axial distances of the two taps from the boundary layer suction slot at the entrance of the test section.

Two different length Reynolds numbers have been used for plotting the curves. The free stream Reynolds number, Re_x, was based on the average main stream water temperature in the core of the flow. The mean boundary layer Reynolds number, Re_{x_m}, was based on the mean boundary layer temperature; the latter was taken as the average between the wall and main stream temperatures.

With the exception of Figure 9, the data placed on each figure were all obtained during the same day. This was to assure that the runs shown on each graph could be directly compared.

Discussion of the Data

Friction Factor Data

Effect of Dirt Particles on Transition: Figures 9 to 12 illustrate
the performance of the system for a variety of diameter Reynolds numbers
ranging from 115,000 to 167,000, with transition determined from measure-
ments of local apparent friction factor. A predominant characteristic which
the curves display is that, as successive runs were taken, the value of the
transition Reynolds number decreased from a maximum of 300,000 in Figure 9
to 400,000 in Figure 11. This is especially evident from a comparison of
Figures 10 and 11 which have essentially the same diameter Reynolds numbers
and percent boundary layer suction, but different transition Reynolds
numbers. This characteristic of decreasing transition Reynolds number on
successive days existed throughout the entire period of experimentation,
and was attributed to the collection of fine particles of foreign matter on
the surfaces of the inlet nozzles and test section. This increased the
disturbance level of the system, thereby causing transition to occur earlier.
This conclusion was verified by the fact that the transition point could be
restored to its earlier position by giving the inlet sections and test pipe
a thorough cleaning.

Effect of Heating on Transition: Figures 10, 11, and 12, each contain
two curves, one for adiabatic conditions, and the other with steam supplied
to produce a small temperature difference across the boundary layer. The
curves show that heating caused no appreciable change in the free stream
transition Reynolds number, but that the mean boundary layer transition
Reynolds number was increased slightly.

Data From Boundary Layer Probe

Figure 13 shows the first data taken with the boundary layer probe
immediately after the system had been given a thorough cleaning. It is
noticed that the decrease in disturbance level due to cleaning has doubled
the transition Reynolds number as compared to the previous run.

Effect of Boundary Layer Suction on Transition: Figures 14, 17, 18, 19, and 20 show experimental results for a range of diameter Reynolds numbers from 30,000 to 120,000. For each adiabatic set of curves with constant Re_D there are shown various rates of boundary layer suction flow. These curves illustrate that beyond a certain percentage the suction rate did not have an appreciable effect on the location of transition.

When the boundary layer suction rate was zero, on the other hand, the transition point was displaced considerably upstream. This is partly explained by the fact that the boundary layer formed in the inlet section was not being removed, thereby producing the effect of extending the length of the pipe upstream, and partly by the fact that the boundary layer suction slot itself was causing a disturbance under these circumstances.

Effect of Heating and Accumulation of Foreign Particles on Transition: Compared with the adiabatic curves in Figures 14, 17, 18, 19, and 20, the heating curves exhibit a slightly smaller free stream Reynolds number of transition, but a slightly greater mean boundary layer Reynolds number of transition. The heating curves are also positioned above the adiabatic curves, thus giving evidence that the velocity profile near the wall has been modified by heat transfer.

Throughout this series of runs it may again be noted that there was a continuous decrease in the transition Reynolds number due to the accumulation of dirt and foreign matter in the inlet sections. During the experimental work the location of the transition point remained constant during any particular day. An example of this is shown in Figure 25 where runs 68 and 72 show transition at the same location although one run was taken in the morning and the other late in the afternoon. The transition Re_x appeared to decrease from day to day and especially over week-ends when the drained system was allowed to stand for a few days. This suggests that the foreign matter was probably salts deposited by evaporation of water left within the system. The powdery white deposits found on the

interior surfaces of the system when it was cleaned seemed to be of this nature.

Since it was desirable to eliminate as much as possible the effect of stream disturbances, the system was given another cleaning before obtaining run 60 in Figure 21. This caused the transition Reynolds number to increase to twice the value indicated in Figure 20. Figures 21 and 22 again demonstrate that heating was ineffective in increasing the free stream length Reynolds number of transition, but that the mean boundary layer Reynolds number of transition was slightly increased.

Because the cleaning had only increased the adiabatic transition Reynolds number to about 500,000, it was decided to give the system still another cleaning, as higher values had been reached previously. Before run 64 in Figure 23 was obtained the system had been given a very thorough cleaning and the nozzles, stilling chamber, and test section were brightly polished. The joint between the two contractions was further honed to assure its being especially smooth.

Figures 23 and 24 show the first group of runs taken after cleaning, and it is seen that the adiabatic transition Reynolds number was restored to 850,000. It is also evident that heating produced a rather pronounced decrease in the free stream transition Reynolds number, but a slight increase in the mean boundary layer transition Reynolds number. Figures 25, 26, 27, and 28 show the effects of heating with different temperature gradients across the boundary layer. In all cases heating appeared to cause a small decrease in the free stream transition Reynolds number but an increase in the mean boundary layer transition Reynolds number. The increase in the latter was generally more pronounced as the temperature difference was increased.

The Addition of Detergent to the System: During a previous experimental work in which lucite contraction nozzles were employed in a water flow system, it was observed that tiny air bubbles would adhere to the interior

surfaces of the nozzles and cause large reductions in the transition
Reynolds number due to their effective roughness. In the present apparatus
it was thought that a small accumulation of grease on the nozzle surfaces
would facilitate the adherence of such bubbles and might possibly account
for the observed day to day decrease of transition Reynolds number.
Detergent was therefore added to the water during run 63 to eliminate
any grease film and bubble collection, and in addition to help prevent
the accumulation of dirt particles. Figure 29 shown that the addition of
the detergent was ineffective in displacing the position of transition.

This result does not eliminate the possibility of air bubbles coming
out of solution and remaining in suspension, with the net effect of causing
disturbances which might lead to premature transition.

VI. SIGNIFICANCE OF RESULTS

The results of these experiments have clearly demonstrated that in the case of internal water flows, the length Reynolds number of transition is very strongly dependent upon the stream disturbance level. Even very small deposits of foreign matter along the walls were sufficient to reduce the value of Re_x at transition by fifty percent. Even with special precautions it was difficult to attain values of Re_x at transition as high as 850,000, and in the usual water system of a practical nature it would be difficult to achieve such a low disturbance level.

For values of disturbance level present in this work, corresponding to values of Re_x at transition ranging from 850,000 to 250,000, no increase in the free stream length Reynolds number of transition was observed when heat was applied, and in fact a slight decrease occurred in some instances. However, heating consistently caused an increase in the mean boundary layer length Reynolds number of transition. Since in design work it is the free stream Reynolds number which is physically significant in predicting the location of transition, it can be said that with normal disturbance levels present in practical situations, heating would be of no significance in extending the laminar regime of flow.

These experiments have not conlusively proven that heating is ineffective in delaying transition, for if the stream disturbance level could be sufficiently reduced, then perhaps a heating effect would be realized. However, as shown by the experimental results, it is extremely difficult to obtain streams of sufficiently low turbulence level, and so it is doubtful that heating could be utilized as a practical means for delaying transition except perhaps under unusual circumstances.

At present the mathematical theory of stability has in fact not been developed for the case of liquid flows with heating or cooling, so we can only speculate as to what the results may be by drawing an analogy with the results for air flows. Since for a liquid the behavior of viscosity as a

function of temperature is opposite to that of a gas, it would be expected that the influence of temperature on the shape of the velocity profile in a liquid flow would also be opposite to that of a gas flow. Thus, while heating tends to destabilize a gas flow, we might expect it to cause a liquid flow to become more stable. However, this analogy could only apply for predicting the behavior of the instability point in a stream containing vanishingly small disturbances.

Assuming that the analogy is valid for liquid flows, the present work provides two results: 1) In a practical case where the disturbances are not vanishingly small, their effect may be very significant and perhaps actually govern the process. 2) The results provide additional evidence that in many circumstances it is not possible to extend predictions for the location of the instability point to that of the transition point.

It must be noted that there are really two effects entering when heat is applied to the wall of the test section. One is the change in shape of the velocity profile resulting from the viscosity gradient produced by heating the boundary layer. This may cause an increase or decrease in stability which may in turn change the position of transition. The other is merely the change in the mean viscosity of the boundary layer. When a liquid boundary layer is heated, the mean viscosity decreases, and hence the effective Reynolds number in the layer is increased for the same flow velocity. This per se will tend to cause transition to occur earlier. Evidently, from the experimental results, if stability is increased by heating, the viscosity effect is sufficiently large to compensate and cause the net result to be essentially zero or slightly negative. Actually, in this respect, the mean boundary layer Reynolds number is a better indication of what occurs within the boundary layer itself. The delay in transition in relation to that parameter indicates that an increase in stability was present, although not sufficiently large to be of practical importance.

After the mathematical theory has been investigated for liquids to an

extent comparable to the present knowledge for air, two additional things remain to be determined before comparisons with experiments can be made with a better degree of certainty. First the effect of large disturbances should be dealt with, that is, the non-linear effects of the governing equations must be considered. Secondly, the zone of unstable wave amplification which occupies the interval between the instability point and the transition point should be investigated, including the effect of temperature gradients on amplification. At least a qualitative answer to the latter question is necessary before instability criteria can be correlated with the behavior of transition.

VII. RECOMMENDATIONS FOR FUTURE WORK

If further work is performed with this type of system an improvement would result if the system were completely closed and contained distilled water. This would help prevent dirt and insoluble salts from collecting on the walls of the system, and in addition would eliminate the possible appearance of air bubbles. Since cooling water would not be admitted during the heated runs under these circumstances, refrigeration would be necessary to keep the system temperature from rising.

Since the boundary layer probe proved successful as a means for determining transition, the use of wall pressure taps could be eliminated. This would prevent any possible disturbance that the taps themselves may induce and would also simplify the apparatus construction.

It would be worthwhile to investigate the behavior of the boundary layer under the effect of larger temperature gradients. This could be accomplished by either pressurizing the steam jacket to accommodate high temperature steam, or by maintaining a lower water temperature by the use of refrigeration.

It would be of interest to try cooling the liquid boundary layer. In this instance the increase of viscosity in the boundary layer produces the effect of decreasing the Reynolds number in that region, and this would tend to move transition downstream. On the other hand, the boundary layer velocity profile would tend to develop an inflection, thus becoming more unstable.

VIII. FRICTION FACTOR IN THE LAMINAR ENTRY OF A SMOOTH PIPE

Brief Summary of Previous Work

Various theories predicting the behavior of the boundary layer for adiabatic, incompressible flow in the laminar entry of a tube have been formulated by Boussinesq[1], Schiller[16], and Langhaar[7]. Atkinson and Goldstein[5] have solved the differential equations by use of series expansions and found expressions valid near the entrance of the pipe. This solution was then joined to a second expression, valid at larger distances from the entrance, derived from an extension of the method used by Boussinesq. A simple theory, using momentum integral methods, has been derived by Kline and Shapiro[6] for the region where the boundary layer is very thin. They also present a set of curves comparing the calculated results for all these methods with their experimental data.

Solution for Region Where δ/R is Very Small

The development of the boundary layer in a tube is complicated by the fact that its formation affects the velocity in the frictionless core of the flow. The resulting acceleration of the core produces a pressure gradient along the pipe which in turn affects the boundary layer formation. The basic physical nature of the process suggests that a method of successive approximations might be used to obtain a solution. In this scheme the continuity equation is applied to obtain an approximation to the core velocity along the tube. The latter is then substituted in the approximate boundary layer calculation method of Thwaites[21], and of Rott and Crabtree[13], to obtain the displacement thickness as a function of distance along the tube. This displacement thickness is then substituted back into the continuity relation to obtain a better approximation to the core velocity, and the whole operation is repeated.

The calculations, as carried out in Appendix C, result in the expression,

$$4\bar{f}_{APP} \frac{X}{D} = 13.76 \frac{\sqrt{Re_x}}{Re_D}\left[1 - 2.88 \frac{\sqrt{Re_x}}{Re_D} + 111 \frac{Re_x}{Re_D^2} - \cdots\right]$$

which is valid in the range where Re_x/Re_D^2 is less than 10^{-3}, within which good convergence is obtained. For Re_x/Re_D^2 equal to 10^{-3}, δ/R is approximately 0.3.

For values larger than 10^{-3} the boundary layer has become so thick that three dimensional effects enter and the method breaks down. Also since the solution has not been constrained to converge eventually to a fully-developed laminar profile it would be expected to be valid only in the entry region of the pipe where the boundary layer is still relatively thin compared to the pipe diameter. A comparison of the computed values with experimental data is shown in Figure 30.

Solution for Entire Laminar Entry Region

A second solution for the apparent friction factor in a laminar tube entry was obtained by substituting an approximate expression for the velocity profile into the equations of continuity and momentum. The profile chosen was in the form u/U = Function $\left[(y/\delta), (\delta/R)\right]$, and was constrained to approach a parabolic shape as the boundary layer thickness became equal to the tube radius. This method yielded a solution which applies throughout the whole entry region, and is in close agreement with both the experimental data of Kline and Shapiro[6] and with the expression stated in the preceding paragraph. The computations are fully explained in Appendix D, and the results are shown in Figures 31 to 34.

IX. CONCLUSIONS

1. For disturbance levels producing length Reynolds numbers of transition up to 850,000, the extent of the laminar regime for water flowing in a pipe entry was found to be either unaffected or slightly decreased when the pipe walls were heated.

2. The length Reynolds number of transition for water flows was found to be very sensitive to small disturbances such as might be caused by small roughnesses on the walls.

3. Heating caused small increases in the mean boundary layer length Reynolds number of transition, which indicates an increased stability. However, the increases produced were not sufficiently large to be of practical importance.

4. There is need for further mathematical study of the unstable wave amplification which follows the instability point and induces turbulence, before a clear understanding of the relation between the instability and transition points can be obtained.

REFERENCES

1. Boussinesq, J., "Hydrodynamique," Comptes Rendus, Vol. 110, 1890, pp. 1160-1238; Vol. 113, 1891, pp. 9-49.

2. Dryden, H. L. and Abbot, I. H., "The Design of Low-Turbulence Wind Tunnels," NACA T. N. No. 1755, Nov. 1948.

3. Dryden, H. L. and Schubauer, G. B., "The Use of Damping Screens for the Reduction of Wind-Tunnel Turbulence," Journal of the Aero. Sci., Vol, 14, April 1947, pp. 221-228.

4. Eckert, B. and Pfluger, F., "The Resistance Coefficient of Commercial Round Wire Grids," NACA T. M. No. 1003, Jan. 1942.

5. Goldstein, S., Modern Developments in Fluid Dynamics, Oxford University Press, 1938.

6. Kline, S. J. and Shapiro, A. H., "The Effect of Cooling on Boundary Layer Transition in a Gas," Final Report on DIC Project 3-6927 at M.I.T. Submitted to NACA under Contract NAw-6125, Sept. 30, 1952.

7. Langhaar, H., "Steady Flow in the Transition Length of a Straight Tube," Journal of Applied Mech., Vol. 9, No. 2, June 1942, pp. A-55 to A-58.

8. Lees, L., "The Stability of the Laminar Boundary Layer in a Compressible Fluid," NACA Report No. 876, 1947.

9. Lees, L. and Lin, C. C., "Investigation of the Stability of the Laminar Boundary Layer in a Compressible Fluid," NACA T. N. No. 1115, Sept. 1946.

10. Liepmann, H. W. and Fila, G., "Investigations of Effects of Surface Temperature and Single Roughness Elements on Boundary Layer Transition," NACA T. N. No. 1196, April 1947.

11. Lin, C. C., "On the Stability of Two-Dimensional Parallel Flows," Quarterly of App. Math., Part I, Vol. III, No. 2, July 1945, pp. 117-142; Part II, Vol. III, No. 3, Oct. 1945, pp. 218-234; Part III, Vol. III, No. 4, Jan. 1946, pp. 277-301.

12. McCullough, G. B. and Gault, D. E., "An Experimental Investigation of the NACA 63_1-012 Airfoil Section with Leading-Edge and Midchord Suction Slots," NACA T. N. 2041, Feb. 1950.

13. Rott, N. and Crabtree, L. F., "Simplified Laminar Boundary-Layer Calculations for Bodies of Revolution and for Yawed Wings," Journal of the Aero Sci., Vol. 19, No. 8, Aug. 1952.

14. Rouse, H. and Hassan, M. M., "Cavitation-Free Inlets and Contractions," Mechanical Engineering, Vol. 71, No. 3, March 1949, pp. 213-216.

15. Scherrer, R., "Boundary-Layer Transition on a Cooled 20° Cone at Mach Numbers of 1.5 and 2.0," NACA T. N. No. 2131, July 1950.

16. Schiller, L., "Die Entwicklung der Laminaren Geschwindigkeitverteilung und ihre Bedeutung fur Zahigkeitsmessungen," _Zeitschrift fur Angewandte Mathematic und Mechanik_, Vol. 2, 1922, p. 96.

17. Schlichting, H., "Amplitudenverteilung und Enerbilanz der kleinen Storungen bei der Plattenstromung," _Nachr. d. Ges. d. Wiss. zu Gottingen_, Math. Phys. Kl., Neue Folge, Bd. 1, Nr. 4, 1935, pp. 47-48.

18. Schlichting, H., _Grenzschicht-Theorie_, Karlsruhe: Verlag G. Braun, 1951.

19. Schubauer, G. B. and Skramstad, H. K., "Laminar-Boundary Layer Oscillations and Transition on a Flat Plate," _NACA Report No. 909_, 1948.

20. Schubauer, G. B., Spangenberg, W. G., and Kebanoff, P. S., "Aerodynamic Characteristics of Damping Screens," _NACA T. N. No. 2001_, Jan. 1950.

21. Thwaites, B., "Approximate Calculation of the Laminar Boundary Layer," _The Aeronautical Quarterly of the Royal Aero. Soc._, Vol. 1, Nov. 1949, pp. 245-280.

22. Tollmien, W., "Uber die Entstehung der Turbulenz," _Nachr. d. Ges. d. Wiss. zu Gottingen_, Math-Physik Kl., 1929, pp. 21-44. (translated as _NACA T. M. No. 609_, 1931.)

23. Tollmien, W., "Ein allgemeines Kriterium der Instabilitat Laminarer Geschwindigkeitverteilungen," _Nachr. d. Ges. d. Wiss. zu Gottingen_, Math-Physik Kl., Neue Folge, Bd. 1, Nr. 5, 1935, pp. 79-144. (translated as _NACA T. M. No. 792_, 1936.)

24. Van Dreist, E. R., "Calculation of the Stability of the Laminar Boundary Layer in a Compressible Fluid on a Flat Plate with Heat Transfer," _Journal of the Aero. Sci._, Vol. 19, No. 12, Dec. 1952, pp. 801-812.

25. "Fluid Meters, Their Theory and Application," _ASME Research Publication_, Fourth Edition, 1937.

LIST OF SYMBOLS

A   cross sectional area of the test tube

D   diameter of the test tube

$4f_{APP}$ local apparent friction factor as defined by the equation:

$$4f_{APP} = \frac{dp/d(x/D)}{\frac{1}{2}\rho v^2}$$

$4\bar{f}_{APP}$ mean apparent friction factor up to a section x = L, defined by the equation:

$$4\bar{f}_{APP}\left(\frac{L}{D}\right) \equiv \int_0^{L/D} 4f_{APP}\, d\left(\frac{x}{D}\right) = \frac{p_{x=0} - p_{x=L}}{\frac{1}{2}\rho V^2}$$

H   the ratio of δ^* to θ

m   a parameter in Thwaites' method defined by:

$$m = -\frac{U'\theta^2}{\nu} \qquad U' = \frac{dU}{dx}$$

p_{STATIC} ⎫
p ⎬   static pressure in the test section at distance x from the boundary layer suction slot

p_{TOTAL} total pressure at x in the boundary layer at a fixed small distance from the tube wall

Q   volume rate of flow through the test section

R   pipe radius

r   radial coordinate in the test section measured from the tube axis

Re_D diameter Reynolds number based on the diameter of the test section and on the free stream fluid properties, $\rho_0 VD/\mu_0$

Re_x length Reynolds number based on the length from the boundary layer suction slot and on the free stream properties, $\rho_0 Vx/\mu_0$

Re_{x_m} length Reynolds number based on the length from the boundary layer suction slot and on fluid properties taken at the average of the free stream and wall temperatures, $\rho_m Vx/\mu_m$

T_0 free stream water temperature in the test section

T_w wall temperature of the test section

U   velocity in the frictionless core of the pipe flow

U_∞	main stream velocity for flow over a flat plate
u	axial velocity at any location x and y
V	mean flow velocity through the test section, Q/A
x	axial distance in the test section measured from the boundary layer suction slot
y	radial coordinate in the test section measured from the wall
α_1	a constant
β_1	a constant
δ	boundary layer thickness
δ^*	displacement thickness of the boundary layer
θ	momentum thickness of the boundary layer
λ	Pohlhausen form parameter defined by the equation:

$$\lambda = \frac{\delta^2}{\nu}\frac{dU}{dx}$$

μ	coefficient of viscosity
ν	kinematic viscosity, μ/ρ
ρ	mass density
σ	dimensionless length parameter, Re_x/Re_D^2
τ_w	shear stress at the wall

TABLE I

LOCATION OF STATIC PRESSURE TAPS
ALONG TEST SECTION

Tap Number	Distance From Suction Slot
	inches
1	1 1/4
2	3
3	5
4	7
5	9
6	11
7	13
8	15
9	18
10	21
11	25
12	29
13	34
14	40
15	48
16	57
17	68
18	80

TABLE II

THERMOCOUPLE LOCATIONS

Thermocouple Number	Location
1	Interior of honeycomb.
2	Boundary layer suction collection header.
3	Wall of the small contraction nozzle.
4	Wall of test section, 2" from suction slot.
5	Wall of test section, 8" from suction slot.
6	Wall of test section, 14" from suction slot.
7	Wall of test section, 24" from suction slot.
8	Wall of test section, 41" from suction slot.
9	Wall of test section, 70" from suction slot.
10	Test section exit.

APPENDIX A

Analysis of Data

The flow in the main pipe line leading to the test section and boundary layer suction slot, and the flow in the boundary layer suction were both calculated from the pressure drop across standard sharp edge orifice plates. The orifice coefficients used were obtained from the tables of values supplied by the ASME in reference 25.

The flow in the test section was taken to be equal to the main line flow minus the flow removed by boundary layer suction.

The free stream length Reynolds number was calculated from the relation, $Re_x = \dfrac{Vx\rho}{\mu}$, where ρ and μ were taken at the free stream temperature. In the case of a heated run this was obtained as the average of the inlet and exit temperatures of the test section. When calculating the mean boundary layer Reynolds number the properties were selected at a temperature equal to the average between the wall temperature and the free stream temperature, the wall temperature being taken as the average of the wall thermocouple readings. For the friction factor data the mean value of x between two pressure taps in the laminar zone was taken, as suggested in reference 6, as the average of the arithmetic and geometric means of the axial distances of the two taps from the boundary layer suction slot at the entrance of the test section.

The local apparent friction factor between two pressure taps was obtained from the formula,

$$4f_{APP} = \frac{\Delta p/\Delta(x/D)}{\frac{1}{2}\rho V^2}$$

where Δp is the static pressure change, and $\Delta(x/D)$ is the number of diameters between the two taps.

The values of $P_{TOTAL} - P_{STATIC}$ were obtained directly from the manometers as the difference of two readings.

APPENDIX B

Approximate Calculation of Experimental Curve Obtained by the Boundary Layer Probe in the Laminar Zone

To obtain an approximate idea of the shape of curve obtained by the boundary layer probe in the laminar zone, a velocity profile for flat plate flow was selected from Schlichting[18] (page 191). Since near the entry of the test section the boundary layer is thin, a flat plate approximation, neglecting the effects of cross-section curvature and pressure gradients along the flow, was sufficiently accurate for this computation.

The velocity profile selected was

$$\frac{u}{U_\infty} = 2\left(\frac{y}{\delta}\right) - 2\left(\frac{y}{\delta}\right)^3 + \left(\frac{y}{\delta}\right)^4 \tag{1}$$

where

$$\delta(x) = \sqrt{\frac{2\beta_1}{\alpha_1}}\sqrt{\frac{\nu x}{U_\infty}} \qquad \begin{array}{l} \text{with} \quad \beta_1 = 2 \\ \text{and} \quad \alpha_1 = \frac{37}{315} \end{array} \tag{2}$$

In the case of flow in a pipe entry, $U_\infty = U$, and the value of U changes as the flow develops along the pipe length. In the present example, since the boundary layer is thin, U can be considered as a first approximation equal to V, the mean velocity in the tube. Then (2) reduces to

$$\delta(x) = \frac{5.84x}{\sqrt{Re_x}} \qquad \text{where} \quad Re_x = \frac{Vx}{\nu} \tag{3}$$

Since the dynamic pressure at a fixed distance from the wall is proportional to u^2, we obtain from (1),

$$\left(\frac{u}{V}\right)^2 = 4\left(\frac{y}{\delta}\right)^2 - 8\left(\frac{y}{\delta}\right)^4 + 4\left(\frac{y}{\delta}\right)^5 + 4\left(\frac{y}{\delta}\right)^6 - 4\left(\frac{y}{\delta}\right)^7 + \left(\frac{y}{\delta}\right)^8 \tag{4}$$

Substituting (3) into (4) results in

$$\left(\frac{u}{V}\right)^2 = \frac{4y^2}{\left[\frac{5.84x}{\sqrt{Re_x}}\right]^2} - \frac{8y^4}{\left[\frac{5.84x}{\sqrt{Re_x}}\right]^4} + \frac{4y^5}{\left[\frac{5.84x}{\sqrt{Re_x}}\right]^5} + \frac{4y^6}{\left[\frac{5.84x}{\sqrt{Re_x}}\right]^6} - \frac{4y^7}{\left[\frac{5.84x}{\sqrt{Re_x}}\right]^7} + \frac{y^8}{\left[\frac{5.84x}{\sqrt{Re_x}}\right]^8} \tag{5}$$

Simplification and rearrangement then produces the final form

$$\left(\frac{u}{V}\right)^2 = \frac{\left[\left(\frac{y}{x}\right)\left(\frac{y}{D}\right)Re_D\right]}{8.53} - \frac{\left[\left(\frac{y}{x}\right)\left(\frac{y}{D}\right)Re_D\right]^2}{1.45} + \frac{\left[\left(\frac{y}{x}\right)\left(\frac{y}{D}\right)Re_D\right]^{5/2}}{1700}$$

$$+ \frac{\left[\left(\frac{y}{x}\right)\left(\frac{y}{D}\right)Re_D\right]^3}{9920} - \frac{\left[\left(\frac{y}{x}\right)\left(\frac{y}{D}\right)Re_D\right]^{7/2}}{57,900} + \frac{\left[\left(\frac{y}{x}\right)\left(\frac{y}{D}\right)Re_D\right]^4}{1,350,000}$$

(6)

Numerical Example

Since the experimental probe used had a finite width, the dynamic pressure indicated was actually an average value over a certain thickness of the boundary layer. To simplify the calculations a fixed value of $y = 0.020$ inches was used, which is in the neighborhood of the actual probe size. Other typical values assumed were:

$$Re_D = 100,000 \qquad D = 2'' \qquad T_o = 75°F$$

and

$$V = \frac{Re_D \, \nu}{D} = 21,400 \text{ ft/hr}$$

or

$$V^2 = 35.3 \text{ ft}^2/\text{sec}^2$$

Then from (6), u^2 was calculated at each value of x, for which the values $P_{TOTAL} - P_{STATIC} = u^2/2g$ were found at each point where $Re_x = Re_D(x/D)$.
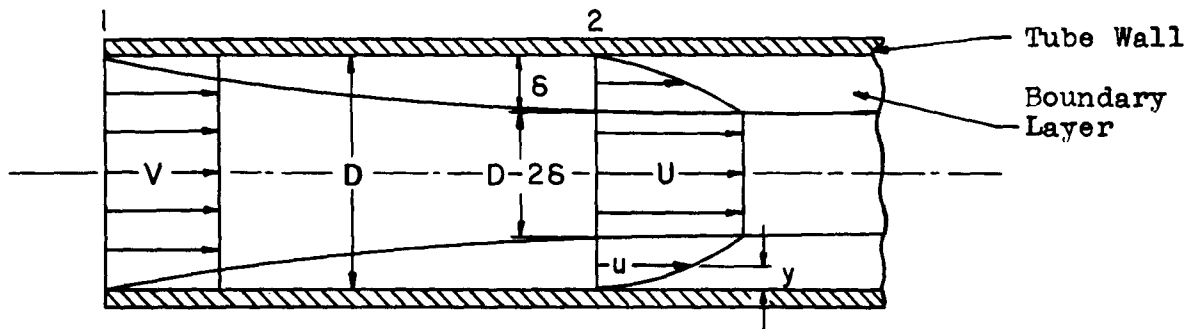
The final results are shown in Figure 6, where the values of $P_{TOTAL} - P_{STATIC}$ have been plotted against Re_x.

APPENDIX C

Determination of an Approximate Expression for $4\bar{\tau}_{APP}$ in the Laminar Entry of a Tube When the Boundary Layer Thickness is Small Compared With the Tube Radius

In this section an expression for $4\bar{\tau}_{APP}$ in the laminar entrance of a tube is derived which applies for values of $\sigma \equiv Re_x/Re_D^2$ less than 10^{-3}. A form of the continuity equation is first obtained by considering the physical situation which exists in the laminar entry. The equation is then integrated by using Pohlhausen's approximate velocity profile, and put into a form where V/U is a function of δ^*/D and dU/dx. Successive approximations of U as a function of x are obtained from this relation and are used with Thwaites'[21] approximate method of laminar boundary layer calculation to obtain higher order approximations. The calculations proceed as follows:

Continuity Relation

Assuming steady flow and applying the continuity equation for a control volume between sections 1 and 2, we obtain the expression,

$$\frac{\pi}{4} D^2 V = \frac{\pi}{4}(D-2\delta)^2 U + \pi \int_0^\delta (D-2y)\, u\, dy \qquad (1)$$

Simplifying, we get

$$\frac{V}{U} = 1 - 4\left(\frac{\delta}{D}\right) + 4\left(\frac{\delta}{D}\right)^2 + \frac{4}{UD}\int_0^\delta u\, dy - \frac{8}{UD^2}\int_0^\delta y u\, dy$$

This is equivalent to

$$\frac{V}{U} = 1 - 4\int_0^\delta \frac{1}{D}\, dy + \frac{8}{D^2}\int_0^\delta y\, dy + \frac{4}{UD}\int_0^\delta u\, dy - \frac{8}{UD^2}\int_0^\delta y u\, dy$$

Regrouping of the integrals results in the expression

$$\frac{V}{U} = 1 - \frac{4}{D}\int_0^\delta \left(1 - \frac{u}{U}\right) dy + \frac{8}{D^2}\int_0^\delta \left(1 - \frac{u}{U}\right) y \, dy$$

Introducing the definition of displacement thickness,

$$\delta^* = \int_0^\delta \left(1 - \frac{u}{U}\right) dy$$

we obtain

$$\frac{V}{U} = 1 - 4\frac{\delta^*}{D} + \frac{8}{D^2}\int_0^\delta \left(1 - \frac{u}{U}\right) y \, dy \tag{2}$$

To evaluate the last term in (2) a velocity distribution u/U as a function of y must be assumed. A good assumption is a polynomial of the fourth order due to Pohlhausen[18],

$$\frac{u}{U} = \left[2\left(\frac{y}{\delta}\right) - 2\left(\frac{y}{\delta}\right)^3 + \left(\frac{y}{\delta}\right)^4\right] + \frac{\lambda}{6}\left[\left(\frac{y}{\delta}\right) - 3\left(\frac{y}{\delta}\right)^2 + 3\left(\frac{y}{\delta}\right)^3 - \left(\frac{y}{\delta}\right)^4\right] \tag{3a}$$

where

$$\lambda = \frac{\delta^2}{\nu}\frac{dU}{dx} \qquad \text{and} \qquad \frac{\delta^*}{\delta} = \frac{3}{10} - \frac{\lambda}{120} \tag{3b,c}$$

Substituting (3a) into (2), and integrating the latter, we obtain

$$\frac{V}{U} = 1 - 4\frac{\delta^*}{D} + \frac{8}{15}\frac{\delta^2}{D^2} - \frac{\lambda}{45}\frac{\delta^2}{D^2} \tag{4}$$

Then, from (3c), solving for δ^2 in terms of δ^* and λ, we get

$$\delta^2 = \frac{100\,\delta^{*2}}{9 - \frac{\lambda}{2} + \frac{\lambda}{144}} = \frac{100}{9}\delta^{*2} + \frac{50}{81}\delta^{*2}\lambda + \frac{75}{36\times81}\delta^{*2}\lambda^2 + \cdots \tag{5}$$

If the expressions (5) and (3b) for δ^2 and λ are now inserted into the integrated continuity equation (4), the latter can be reduced to the form

$$\frac{V}{U} = 1 - 4\frac{\delta^*}{D} + \frac{160}{27}\left(\frac{\delta^*}{D}\right)^2 + \frac{2000}{2187}\left(\frac{\delta^*}{D}\right)^2 \frac{\delta^{*2}}{\nu}\frac{dU}{dx} + \cdots \tag{6}$$

1st Iteration

To begin the iteration process, an expression for the core velocity U as a function of x is needed. As a first approximation the potential flow solution for flow in a pipe is assumed, that is U = V, or V/U = 1.

It is noted that this is merely the first order term in the continuity
relation (6). If we substitute this into Thwaites' expression for the
square of the momentum thickness

$$\theta^2 = .45 \, U^{-6} \, \nu \int_0^x U^5 \, dx \tag{7}$$

we have

$$\theta^2 = \frac{.45 \, \nu \, x}{V} \tag{8}$$

Continuing with Thwaites' method,

$$m = -\frac{U' \theta^2}{\nu} = 0 \qquad \text{as } U' = 0 \text{ for this} \atop \text{1st approximation} \tag{9}$$

Also, from Thwaites' method

$$\delta^* = \theta \, H(m) \tag{10}$$

By plotting H vs. m as given in table I in reference 21, the relationship
H = H(m) can be approximated in the region of decreasing pressure by the
straight line,

$$H(m) = 2.48m + 2.56 \tag{11}$$

Then putting (8), (9), and (11) into (10) we have,

$$\delta^* = \left[.45 \frac{\nu x}{V} \right]^{1/2} (2.56) = 1.72 \frac{x}{\sqrt{Re_x}} \tag{12}$$

which is the final result of the 1st iteration. It is noted that this
expression is the same as that obtained in the Blasius solution for flow
over a flat plate. This might have been anticipated, as very close to the
entry of the pipe the boundary layer is so thin compared with the tube
radius that it approximates flat plate behavior.

2nd Iteration

We now take as a closer approximation the first two terms from the
continuity relationship (6),

$$\frac{V}{U} = 1 - 4\frac{\delta^*}{D} \quad ; \quad \text{OR} \quad \frac{U}{V} = 1 + 4\frac{\delta^*}{D} + \cdots$$

Substituting δ^* from (12) into (6) we have

$$\frac{U}{V} = 1 + 6.88 \frac{x/D}{\sqrt{Re_x}} = 1 + 6.88 \frac{\sqrt{Re_x}}{Re_D} \tag{13}$$

This expression is then inserted into equation (7), thus yielding

$$\theta^2 = .45 \left[1 + 6.88 \frac{\sqrt{Re_x}}{Re_D} \right]^{-6} \frac{\nu}{V} \int_0^x \left[1 + 6.88 \frac{\sqrt{Re_x}}{Re_D} \right]^5 dx$$

Expanding the terms in square brackets by means of the binomial theorem, and integrating, we get

$$\theta^2 = .45 \left[1 - 41.28 \frac{\sqrt{Re_x}}{Re_D} + \cdots \right] \frac{\nu}{V} \left[x + 22.93 \, x \frac{\sqrt{Re_x}}{Re_D} + \cdots \right]$$

or

$$\theta^2 = .45 \frac{\nu x}{V} \left[1 - 18.35 \frac{\sqrt{Re_x}}{Re_D} + \cdots \right] \tag{14}$$

From (9), (13), and (14) we have

$$m = -\frac{U'\theta^2}{\nu} = \frac{\left[-3.44 \frac{V}{x} \frac{\sqrt{Re_x}}{Re_D} \right] \left[.45 \frac{\nu x}{V} \left(1 - 18.55 \frac{\sqrt{Re_x}}{Re_D} \right) \right]}{\nu}$$

or

$$m = -1.55 \frac{\sqrt{Re_x}}{Re_D} \left[1 - 18.35 \frac{\sqrt{Re_x}}{Re_D} + \cdots \right] \tag{15}$$

From (10) and (11),

$$\delta^* = \theta \left(2.48m + 2.56 \right) \tag{16}$$

Substituting (14) and (15) into (16) and retaining only terms up to order $\sqrt{Re_x}/Re_D$, there is obtained

$$\delta^* = \left[.45 \frac{\nu x}{V} \right]^{1/2} \left[1 - 9.18 \frac{\sqrt{Re_x}}{Re_D} \right] \left\{ 2.48 \left[-1.55 \frac{\sqrt{Re_x}}{Re_D} \left(1 - 18.35 \frac{\sqrt{Re_x}}{Re_D} \right) \right] + 2.56 \right\}$$

or

$$\delta^* = \frac{1.72 \, x}{\sqrt{Re_x}} \left[1 - 10.68 \frac{\sqrt{Re_x}}{Re_D} \right] \tag{17}$$

This is the final result of the 2nd iteration.

3rd Iteration

We now take as a closer approximation the first three terms from the continuity relation (6), and proceed in the same manner as before:

$$\frac{V}{U} = 1 - 4\frac{\delta^*}{D} + \frac{160}{27}\left(\frac{\delta^*}{D}\right)^2 \tag{18}$$

Substituting (17) for δ^* into (18), and simplifying, we obtain

$$\frac{V}{U} = 1 - 6.88\frac{\sqrt{Re_x}}{Re_D} + 91.1\frac{Re_x}{Re_D^2} + \cdots$$

or

$$\frac{U}{V} = 1 + 6.88\frac{\sqrt{Re_x}}{Re_D} - 43.7\frac{Re_x}{Re_D^2} + \cdots \tag{19}$$

which is the same as (13), except that we have retained the next higher order term.

Equation 19 is now inserted into (7) with the result, after integration, simplification, and dropping of all terms of order higher than Re_x/Re_D^2, that

$$\frac{\theta^2}{x^2} = \frac{.45}{\sqrt{Re_x}}\left[1 - 18.35\frac{\sqrt{Re_x}}{Re_D} + 439\frac{Re_x}{Re_D^2}\right] \tag{20}$$

From Eqs. (9), (19), and (20), we have

$$m = -.45\left[3.44\frac{\sqrt{Re_x}}{Re_D} - 106.9\frac{Re_x}{Re_D^2}\right] \tag{21}$$

Solving for δ^* from Eqs. (10), (11), (20), and (21), we have, after simplification,

$$\delta^* = \frac{1.72x}{\sqrt{Re_x}}\left[1 - 10.68\frac{\sqrt{Re_x}}{Re_D} + 238\frac{Re_x}{Re_D^2}\right] \tag{22}$$

Now we insert (22) and dU/dx from (19) into the first four terms of the continuity equation (6), and thus we obtain

$$\frac{V}{U} = 1 - 4\frac{\delta^*}{D} + \frac{160}{27}\left(\frac{\delta^*}{D}\right)^2 + \frac{2000}{2187}\left(\frac{\delta^*}{D}\right)^2\frac{\delta^{*2}}{\nu}\frac{dU}{dx}$$

with the result that

$$\frac{V}{U} = 1 - 6.88\frac{\sqrt{Re_x}}{Re_D} + 90.9\frac{Re_x}{Re_D^2} - 1986\frac{Re_x^{3/2}}{Re_D^3} + \cdots$$

or

$$\frac{U}{V} = 1 + 6.88 \frac{\sqrt{Re_x}}{Re_D} - 43.5 \frac{Re_x}{Re_D^2} + 1060 \frac{Re_x^{3/2}}{Re_D^3} - \cdots \qquad (23)$$

It is noticed that the successive coefficients in the series grow quite rapidly and thus good convergence is obtained only in the region where Re_x/Re_D^2 is small and less than 10^{-3}. A similar expression was obtained by Atkinson and Goldstein (see reference 5, pages 305-306), their result being

$$\frac{U}{V} = 1 + 6.883 \frac{\sqrt{Re_x}}{Re_D} - 36.375 \frac{Re_x}{Re_D^2} + 1135.86 \frac{Re_x^{3/2}}{Re_D^3} - \cdots$$

We may now write the Bernoulli equation for the frictionless core of the flow between sections 1 and 2 in the figure on page 36. Thus,

$$\frac{p_1 - p_2}{\frac{1}{2}\rho V^2} = \left(\frac{U}{V}\right)^2 - 1$$

where p_1 and p_2 are the static pressures across the whole cross-section at 1 and 2 respectively. Therefore, from the definition of $4\bar{f}_{APP}$,

$$4\bar{f}_{APP} \frac{x}{D} = \left(\frac{U}{V}\right)^2 - 1 \qquad (24)$$

Putting (23) into (24), we have the final result,

$$4\bar{f}_{APP} \frac{x}{D} = 13.76 \frac{\sqrt{Re_x}}{Re_D} \left[1 - 2.88 \frac{\sqrt{Re_x}}{Re_D} + 111 \frac{Re_x}{Re_D^2} - \cdots \right] \qquad (25)$$

A comparison of points calculated from this relation with the experimental curve obtained by Kline and Shapiro[6] is shown in Figure 30.

APPENDIX D

Friction Factor in the Laminar Inlet
of a Smooth Tube Up to the Point of Formation
of Poiseuille Flow

Form of the Boundary Layer Velocity Profile

As discussed previously in section VIII, the determination of the growth of a laminar boundary layer in the entry of a tube is complicated by the fact that the boundary layer growth affects the velocity in the frictionless core of the flow. The growth of the layer produces an acceleration of the core velocity, thus causing a pressure gradient to exist in the flow direction. This in turn affects the boundary layer growth. Since, for a given flow, the core velocity (and hence the pressure) at a particular position along the tube is dependent on the thickness of the boundary layer in relation to the pipe radius, we might expect that the boundary layer velocity profile would also depend upon this ratio. Thus in the case of pipe flow we might say that,

$$\frac{u}{U} = \text{Function} \left[\left(\frac{y}{\delta} \right), \left(\frac{\delta}{R} \right) \right]$$

We may then assume that u/U is of the form,

$$\frac{u}{U} = a_0 + a_1\left(\frac{y}{\delta}\right) + a_2\left(\frac{y}{\delta}\right)^2 + \cdots + b_1\left(\frac{\delta}{R}\right) + b_2\left(\frac{\delta}{R}\right)^2 + \cdots$$
$$+ c_{11}\left(\frac{y}{\delta}\right)\left(\frac{\delta}{R}\right) + c_{12}\left(\frac{y}{\delta}\right)\left(\frac{\delta}{R}\right)^2 + c_{21}\left(\frac{y}{\delta}\right)^2\left(\frac{\delta}{R}\right) + \cdots \tag{1}$$

where a_0, a_1, b_1, b_2, c_{11}, c_{12}, etc., are constants. For the sake of simplicity we shall retain only terms up through the fourth order, and therefore we choose a polynomial for the velocity profile in the form

$$\frac{u}{U} = a_0 + a_1\left(\frac{y}{\delta}\right) + a_2\left(\frac{y}{\delta}\right)^2 + a_3\left(\frac{y}{\delta}\right)^3 + a_4\left(\frac{y}{\delta}\right)^4 + b_1\left(\frac{\delta}{R}\right) + b_2\left(\frac{\delta}{R}\right)^2 + b_3\left(\frac{\delta}{R}\right)^3 + b_4\left(\frac{\delta}{R}\right)^4$$
$$+ c_{11}\left(\frac{y}{\delta}\right)\left(\frac{\delta}{R}\right) + c_{12}\left(\frac{y}{\delta}\right)\left(\frac{\delta}{R}\right)^2 + c_{13}\left(\frac{y}{\delta}\right)\left(\frac{\delta}{R}\right)^3 + c_{21}\left(\frac{y}{\delta}\right)^2\left(\frac{\delta}{R}\right) + c_{22}\left(\frac{y}{\delta}\right)^2\left(\frac{\delta}{R}\right)^2 + c_{31}\left(\frac{y}{\delta}\right)^3\left(\frac{\delta}{R}\right) \tag{2}$$

where the constants have to be fixed to satisfy the boundary conditions of the problem.

Boundary Conditions

The first boundary condition to be considered is that, at the wall, the fluid velocity must equal zero. Thus, at $y = 0$: $u = 0$. Inserting this condition into (2) we have

$$0 = a_0 + b_1\left(\frac{\delta}{R}\right) + b_2\left(\frac{\delta}{R}\right)^2 + b_3\left(\frac{\delta}{R}\right)^3 + b_4\left(\frac{\delta}{R}\right)^4 \tag{3}$$

Thus (2) reduces to

$$\frac{u}{U} = a_1\left(\frac{y}{\delta}\right) + a_2\left(\frac{y}{\delta}\right)^2 + a_3\left(\frac{y}{\delta}\right)^3 + a_4\left(\frac{y}{\delta}\right)^4 + C_{11}\left(\frac{y}{\delta}\right)\left(\frac{\delta}{R}\right) + C_{12}\left(\frac{y}{\delta}\right)\left(\frac{\delta}{R}\right)^2$$
$$+ C_{13}\left(\frac{y}{\delta}\right)\left(\frac{\delta}{R}\right)^3 + C_{21}\left(\frac{y}{\delta}\right)^2\left(\frac{\delta}{R}\right) + C_{22}\left(\frac{y}{\delta}\right)^2\left(\frac{\delta}{R}\right)^2 + C_{31}\left(\frac{y}{\delta}\right)^3\left(\frac{\delta}{R}\right) \tag{4}$$

A second boundary condition which we shall impose is that the velocity u at the edge of the boundary layer shall be equal to the core velocity U. Thus, at $y = \delta$: $u = U$. Inserting this into (4) we have

$$1 = a_1 + a_2 + a_3 + a_4 + C_{11}\left(\frac{\delta}{R}\right) + C_{12}\left(\frac{\delta}{R}\right)^2 + C_{13}\left(\frac{\delta}{R}\right)^3 + C_{21}\left(\frac{\delta}{R}\right) + C_{22}\left(\frac{\delta}{R}\right)^2 + C_{31}\left(\frac{\delta}{R}\right) \tag{5}$$

and we obtain the following equations by equating terms containing equal powers of (δ/R):

$$a_1 + a_2 + a_3 + a_4 = 1 \tag{6}$$

$$C_{11} + C_{21} + C_{31} = 0 \tag{7}$$

$$C_{12} + C_{22} = 0 \tag{8}$$

$$C_{13} = 0 \tag{9}$$

The third boundary condition imposed is that, at $y = \delta$: $\partial u/\partial y = 0$. Dropping the c_{13} term according to (9), and differentiating (4), we have

$$\frac{\partial u}{\partial y} = \frac{U}{\delta}\left[a_1 + 2a_2\left(\frac{y}{\delta}\right) + 3a_3\left(\frac{y}{\delta}\right)^2 + 4a_4\left(\frac{y}{\delta}\right)^3 + C_{11}\left(\frac{\delta}{R}\right) + C_{12}\left(\frac{\delta}{R}\right)^2 \right.$$
$$\left. + 2C_{21}\left(\frac{y}{\delta}\right)\left(\frac{\delta}{R}\right) + 2C_{22}\left(\frac{y}{\delta}\right)\left(\frac{\delta}{R}\right)^2 + 3C_{31}\left(\frac{y}{\delta}\right)^2\left(\frac{\delta}{R}\right)\right] \tag{10}$$

Applying the boundary condition leads to

$$0 = a_1 + 2a_2 + 3a_3 + 4a_4 + C_{11}\left(\frac{\delta}{R}\right) + C_{12}\left(\frac{\delta}{R}\right)^2 \tag{11}$$
$$+ 2C_{21}\left(\frac{\delta}{R}\right) + 2C_{22}\left(\frac{\delta}{R}\right)^2 + 3C_{31}\left(\frac{\delta}{R}\right)$$

which provides the additional equations

$$a_1 + 2a_2 + 3a_3 + 4a_4 = 0 \tag{12}$$

$$c_{11} + 2c_{21} + 3c_{31} = 0 \tag{13}$$

$$c_{12} + 2c_{22} = 0 \tag{14}$$

From (8) and (14) we find that c_{12} and c_{22} must each equal zero.

Following the entry region, within which the boundary layer thickness increases and eventually fills the tube, the velocity profile acquires the parabolic shape characteristic of fully-developed laminar flow. Thus we shall impose a fourth boundary condition, which states that when $\delta = R$, the velocity profile assumes the parabolic shape given by

$$\frac{u}{U} = \left[2\left(\frac{y}{\delta}\right) - \left(\frac{y}{\delta}\right)^2 \right] \tag{15}$$

This condition is then applied to equation (4) (from which the terms involving c_{13}, c_{12}, and c_{22}, have already been omitted as they have been found equal to zero) and we obtain

$$2\left(\frac{y}{\delta}\right) - \left(\frac{y}{\delta}\right)^2 = a_1\left(\frac{y}{\delta}\right) + a_2\left(\frac{y}{\delta}\right)^2 + a_3\left(\frac{y}{\delta}\right)^3 + a_4\left(\frac{y}{\delta}\right)^4 + c_{11}\left(\frac{y}{\delta}\right)$$
$$+ c_{21}\left(\frac{y}{\delta}\right)^2 + c_{31}\left(\frac{y}{\delta}\right)^3 \tag{16}$$

Thus we have the equations

$$a_1 + c_{11} = 2 \tag{17}$$

$$a_2 + c_{21} = -1 \tag{18}$$

$$a_3 + c_{31} = 0 \tag{19}$$

$$a_4 = 0 \tag{20}$$

Since a_4 is equal to zero we are finally left with a profile of the form,

$$\frac{u}{U} = a_1\left(\frac{y}{\delta}\right) + a_2\left(\frac{y}{\delta}\right)^2 + a_3\left(\frac{y}{\delta}\right)^3 + c_{11}\left(\frac{y}{\delta}\right)\left(\frac{\delta}{R}\right) + c_{21}\left(\frac{y}{\delta}\right)^2\left(\frac{\delta}{R}\right) + c_{31}\left(\frac{y}{\delta}\right)^3\left(\frac{\delta}{R}\right) \tag{21}$$

which has six unknown constants. It would seem that these could be solved for from the seven equations (6), (7), (12), (13), (17), (18), and (19). These become, after dropping the constants which are equal to zero,

$$a_1 + a_2 + a_3 = 1 \tag{22}$$

$$C_{11} + C_{21} + C_{31} = 0 \tag{23}$$

$$a_1 + 2a_2 + 3a_3 = 0 \tag{24}$$

$$C_{11} + 2C_{21} + 3C_{31} = 0 \tag{25}$$

$$a_1 + C_{11} \quad = 2 \tag{26}$$

$$a_2 + C_{21} \quad = -1 \tag{27}$$

$$a_3 + C_{31} \quad = 0 \tag{28}$$

However, if (26), (27), and (28), are inserted into (22), equation (23) is obtained. Also if (26), (27), and (28), are inserted into (24), then (25) is obtained, so that only the five equations (22), (24), (26), (27), and (28) are independent. Thus one more equation is needed before the constants can be determined. This will be found from a fifth boundary condition derived from the steady-state equation of motion in cylindrical coordinates,

$$u\frac{\partial u}{\partial x} + v\frac{\partial u}{\partial r} = -\frac{1}{\rho}\frac{\partial p}{\partial x} + \nu\left(\frac{\partial^2 u}{\partial r^2} + \frac{1}{r}\frac{\partial u}{\partial r} + \frac{\partial^2 u}{\partial x^2}\right) \tag{29}$$

The boundary condition states that, at the wall, where $y = 0$: $u = 0$ and $v = 0$. We neglect the term $\frac{\partial^2 u}{\partial x^2}$ in the equation as is usual in boundary layer theory, and apply the Bernoulli equation in the frictionless core of the flow to evaluate $\partial p/\partial x$. Thus we have,

$$0 = -\frac{1}{\rho}\frac{\partial p}{\partial x} + \nu\left(\frac{\partial^2 u}{\partial r^2} + \frac{1}{r}\frac{\partial u}{\partial r}\right) \tag{30}$$

with $-\frac{1}{\rho}\frac{\partial p}{\partial x} = U\frac{dU}{dx}$ and $R = r + y$ where R is the pipe radius. Substituting into (30) and keeping in mind that $\frac{\partial u}{\partial r} = -\frac{\partial u}{\partial y}$, we have that at $y = 0$ we must fulfill the condition,

$$\frac{\partial^2 u}{\partial y^2} + \frac{1}{y-R}\frac{\partial u}{\partial y} = -\frac{U}{\nu}\frac{dU}{dx} \tag{31}$$

We now proceed to evaluate the terms in this equation. Differentiating the velocity profile (21) we have,

$$\frac{\partial u}{\partial y} = \frac{U}{\delta}\left[a_1 + 2a_2\left(\frac{y}{\delta}\right) + 3a_3\left(\frac{y}{\delta}\right)^2 + C_{11}\left(\frac{\delta}{R}\right) + 2C_{21}\left(\frac{y}{\delta}\right)\left(\frac{\delta}{R}\right) + 3C_{31}\left(\frac{y}{\delta}\right)^2\left(\frac{\delta}{R}\right)\right] \tag{32}$$

$$\left[\frac{\partial u}{\partial y}\right]_{y=0} = \frac{U}{\delta}\left[a_1 + C_{11}\left(\frac{\delta}{R}\right)\right] \tag{33}$$

and

$$\frac{\partial^2 u}{\partial y^2} = \frac{U}{\delta^2}\left[2a_2 + 6a_3\left(\frac{y}{\delta}\right) + 2C_{21}\left(\frac{\delta}{R}\right) + 6C_{31}\left(\frac{y}{\delta}\right)\left(\frac{\delta}{R}\right)\right] \tag{34}$$

$$\left[\frac{\partial^2 u}{\partial y^2}\right]_{y=0} = \frac{U}{\delta^2}\left[2a_2 + 2C_{21}\left(\frac{\delta}{R}\right)\right] \tag{35}$$

It is next necessary to evaluate the term dU/dx, and this can be obtained from the continuity relationship (Eq. (1), Appendix C). This can be written in the form,

$$\frac{V}{U} = 1 - 2\left(\frac{\delta}{R}\right) + \left(\frac{\delta}{R}\right)^2 + \frac{2}{R}\int_0^\delta \frac{u}{U}\,dy - \frac{2}{R^2}\int_0^\delta \frac{u}{U}\,y\,dy \tag{36}$$
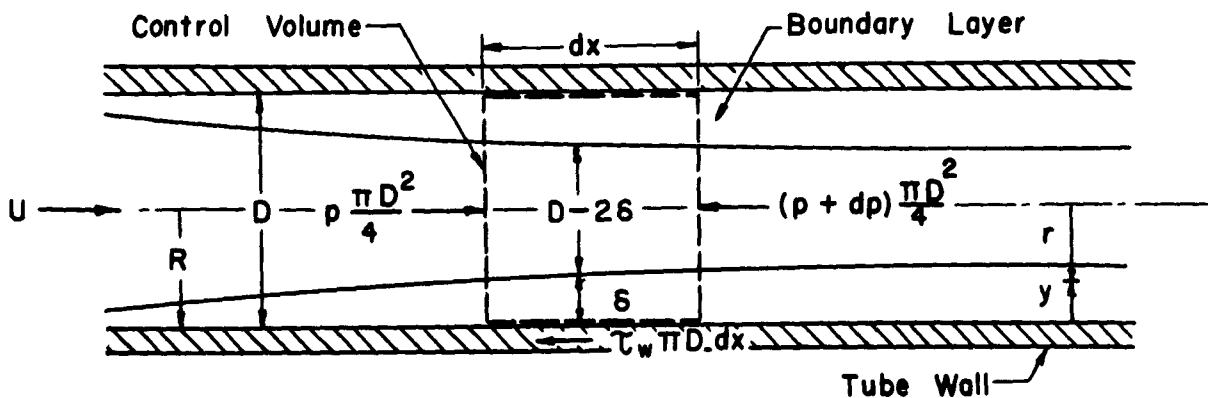
After evaluation of the integrals the equation is solved for U, the result being

$$U = V\Bigg/\left[1 + \left(-2 + a_1 + \frac{2}{3}a_2 + \frac{1}{2}a_3\right)\left(\frac{\delta}{R}\right) + \left(1 + C_{11} + \frac{2}{3}C_{21} + \frac{C_{31}}{2}\right.\right.$$
$$\left.\left. - \frac{2}{3}a_1 - \frac{a_2}{2} - \frac{2}{5}a_3\right)\left(\frac{\delta}{R}\right)^2 + \left(-\frac{2}{3}C_{11} - \frac{1}{2}C_{21} - \frac{2}{5}C_{31}\right)\left(\frac{\delta}{R}\right)^3\right] \tag{37}$$

This can then be differentiated, and dU/dx is found in the form,

$$\frac{dU}{dx} = \left[\text{Function}\left(\frac{\delta}{R}\right)\right]\frac{d\delta}{dx} \tag{38}$$

This then presents the problem that dδ/dx must be evaluated, but once this is found the entire problem is solved after the constants a_1, c_{11}, etc., have been evaluated. To find dδ/dx we must turn to the momentum equation, which may be derived for a tube in momentum-integral form by considering a control volume as shown in the figure below.

If the net force on the control volume is equated to the net outgoing

flux of momentum, we obtain the equation

$$-d p \frac{\pi D^2}{4} - \tau_w \pi D dx = d \left[\int_{cv} \rho u^2 dA \right] = d \left[\int_0^\delta \pi \rho u^2 (D-2y) dy + d \left[\rho \frac{\pi}{4} (D-2\delta)^2 U^2 \right] \right] \tag{39}$$

Applying the Bernoulli equation in the frictionless core to evaluate dp/dx, and using $\tau_w = \mu \left(\frac{\partial u}{\partial y} \right)_{y=0}$, (39) can be reduced to the form

$$U \frac{dU}{dx} - \frac{2\nu}{R} \left(\frac{\partial u}{\partial y} \right)_{y=0} = \frac{2}{R^2} \frac{d}{dx} \left[U^2 \int_0^\delta \frac{u^2}{U^2} (R-y) dy \right] + \frac{d}{dx} \left[\left\{ 1 - 2 \left(\frac{\delta}{R} \right) + \left(\frac{\delta}{R} \right)^2 \right\} U^2 \right] \tag{40}$$

All of the terms in this equation can then be evaluated by the use of the assumed velocity profile (21). The first term on the left hand side and both terms on the right will involve the factor $d\delta/dx$ since these terms contain differentiations with respect to x. The equation can then be solved for $d\delta/dx$ and its value inserted into (38). Equations (33), (35), (37), and (38) are then substituted into the boundary condition (31) and y is set equal to zero. The condition is then examined to attempt to determine the relationship between the undetermined constants so that they may be evaluated. This procedure is extremely long and involves very large algebraic expressions, so it will be omitted from this discussion. The results will be stated and these results will be later verified by substitution into the boundary condition.

It was found impossible to fully satisfy this boundary condition, so it was decided to satisfy it partially. The calculations showed that· the left hand side of (31) had a constant term a_2, with all other terms multiplied by (δ/R) or $(\delta/R)^2$. On the right side, however, no constant term appeared and all terms were multiplied by (δ/R) to the first or a higher power. Thus in order to partially satisfy the boundary condition, a_2 was taken equal to zero. This means that the boundary condition was completely satisfied in the region where (δ/R) is sufficiently small that all terms except the constant term may be neglected. The boundary condition was partially satisfied elsewhere.

With a_2 equal to zero, the constants a_1, a_3, c_{11}, c_{21}, and c_{31} can be

evaluated from equations (22), (24), (26), (27), and (28), resulting in the values

$$a_1 = 3/2, \quad a_2 = 0, \quad a_3 = -1/2, \quad c_{11} = 1/2, \quad c_{21} = -1, \text{ and } c_{31} = 1/2 .$$

Substituting these into equation (21), we have as a final result

$$\frac{u}{U} = \frac{3}{2}\left(\frac{y}{\delta}\right) - \frac{1}{2}\left(\frac{y}{\delta}\right)^3 + \frac{1}{2}\left(\frac{y}{\delta}\right)\left(\frac{\delta}{R}\right) - \left(\frac{y}{\delta}\right)^2\left(\frac{\delta}{R}\right) + \frac{1}{2}\left(\frac{y}{\delta}\right)^3\left(\frac{\delta}{R}\right) \tag{41}$$

To interpret this expression, the terms may be rearranged in the form

$$\frac{u}{U} = \left\{ \left[\frac{3}{2}\left(\frac{y}{\delta}\right) - \frac{1}{2}\left(\frac{y}{\delta}\right)^3\right]\left[1 - \left(\frac{\delta}{R}\right)\right] + \left[2\left(\frac{y}{\delta}\right) - \left(\frac{y}{\delta}\right)^2\right]\left[\frac{\delta}{R}\right] \right\} \tag{42}$$

From this it is seen that as (δ/R) goes to zero, u/U becomes equal to $\left[\frac{3}{2}\left(\frac{y}{\delta}\right) - \frac{1}{2}\left(\frac{y}{\delta}\right)^3\right]$. This is a familar cubic velocity profile for a flat plate (see reference 18, page 191), and thus the profile approaches flat plate behavior when the boundary layer is very thin in comparison with the pipe radius. As (δ/R) goes to one, the first term on the right side goes to zero while the second term increases in magnitude. When (δ/R) is equal to one the profile becomes $u/U = \left[2\left(\frac{y}{\delta}\right) - \left(\frac{y}{\delta}\right)^2\right]$, which is the parabolic profile for fully-developed laminar flow. Thus as (δ/R) goes from zero to one, the shape of the profile gradually changes from a cubic flat plate profile to a fully-developed parabolic profile.

Evaluation of Terms in Continuity and Momentum Equations

Using the approximate velocity profile (41) we will now proceed to solve the continuity and momentum equations to determine the growth of the boundary layer as a function of distance along the tube. Substituting the values of the constants into (37), which has been obtained from the continuity relation, we have

$$U = \frac{V}{\left[1 - \frac{3}{4}\left(\frac{\delta}{R}\right) + \frac{17}{60}\left(\frac{\delta}{R}\right)^2 - \frac{1}{30}\left(\frac{\delta}{R}\right)^3\right]} \tag{43}$$

Differentiation of this expression results in

$$\frac{dU}{dx} = -\frac{V}{R} \frac{\left[-\frac{3}{4} + \frac{17}{30}\left(\frac{\delta}{R}\right) - \frac{1}{10}\left(\frac{\delta}{R}\right)^2\right]\frac{d\delta}{dx}}{\left[1 - \frac{3}{4}\left(\frac{\delta}{R}\right) + \frac{17}{60}\left(\frac{\delta}{R}\right)^2 - \frac{1}{30}\left(\frac{\delta}{R}\right)^3\right]^2} \tag{44}$$

Now, for convenience let

$$A \equiv \left[-\frac{3}{4} + \frac{17}{30}\left(\frac{\delta}{R}\right) - \frac{1}{10}\left(\frac{\delta}{R}\right)^2 \right] \tag{45}$$

$$B \equiv \left[1 - \frac{3}{4}\left(\frac{\delta}{R}\right) + \frac{17}{60}\left(\frac{\delta}{R}\right)^2 - \frac{1}{30}\left(\frac{\delta}{R}\right)^3 \right] \tag{46}$$

The first term in the momentum equation (40) can then be expressed as,

$$U\frac{dU}{dx} = -\frac{V^2}{R}\frac{A}{B^3}\frac{d\delta}{dx} \tag{47}$$

To evaluate the second term in the momentum equation, we determine $\left(\frac{\partial u}{\partial y}\right)_{y=0}$ from equation (33), with the result that

$$\left(\frac{\partial u}{\partial y}\right)_{y=0} = \left[\frac{3}{2} + \frac{1}{2}\left(\frac{\delta}{R}\right) \right]\frac{U}{\delta} \tag{48}$$

Now let

$$E \equiv \left[\frac{3}{2} + \frac{1}{2}\left(\frac{\delta}{R}\right) \right] \tag{49}$$

so that the second term in the momentum equation (40) may be written

$$-\frac{2\nu}{R}\left(\frac{\partial u}{\partial y}\right)_{y=0} = -\frac{2\nu V}{R\delta}\frac{E}{B} \tag{50}$$

Now consider the third term in the momentum equation,

$$\frac{2}{R^2}\frac{d}{dx}\left[U^2 \int_0^\delta \frac{u^2}{U^2}(R-y)\,dy \right] \tag{51}$$

This is differentiated by parts to obtain

$$U^2\frac{d}{dx}\left[\frac{2}{R^2}\int_0^\delta \left(\frac{u}{U}\right)^2(R-y)\,dy \right] + \left[\frac{2}{R^2}\int_0^\delta \left(\frac{u}{U}\right)^2(R-y)\,dy \right]\left[2U\frac{dU}{dx} \right] \tag{52}$$

Evaluating the integral, we have

$$\frac{2}{R^2}\int_0^\delta \left(\frac{u}{U}\right)^2(R-y)\,dy = \left[\frac{34}{35}\left(\frac{\delta}{R}\right) - \frac{1003}{1680}\left(\frac{\delta}{R}\right)^2 - \frac{33}{840}\left(\frac{\delta}{R}\right)^3 - \frac{1}{560}\left(\frac{\delta}{R}\right)^4 \right] \tag{53}$$

Substituting this into (52), introducing U and dU/dx from continuity, and carrying out the differentiation, we obtain

$$\frac{2}{R^2}\frac{d}{dx}\left[U^2\int_0^\delta \left(\frac{u}{U}\right)^2(R-y)\,dy \right] = \left[\frac{V^2}{B^2} \right]\left[\frac{1}{R}\left\{ \frac{34}{35} - \frac{1003}{840}\left(\frac{\delta}{R}\right) - \frac{33}{280}\left(\frac{\delta}{R}\right)^2 - \frac{1}{140}\left(\frac{\delta}{R}\right)^3 \right\} \right]\frac{d\delta}{dx}$$

$$+ \left[\frac{34}{35}\left(\frac{\delta}{R}\right) - \frac{1003}{1680}\left(\frac{\delta}{R}\right)^2 - \frac{33}{840}\left(\frac{\delta}{R}\right)^3 - \frac{1}{560}\left(\frac{\delta}{R}\right)^4 \right]\left[-2\frac{V^2}{R}\frac{A}{B^3} \right]\frac{d\delta}{dx} \tag{54}$$

Now, for convenience, let

$$C \equiv \left[\frac{34}{35} - \frac{1003}{840}\left(\frac{\delta}{R}\right) - \frac{33}{280}\left(\frac{\delta}{R}\right)^2 - \frac{1}{140}\left(\frac{\delta}{R}\right)^3 \right] \tag{55}$$

$$G \equiv \left[\frac{34}{35}\left(\frac{\delta}{R}\right) - \frac{1003}{1680}\left(\frac{\delta}{R}\right)^2 - \frac{33}{840}\left(\frac{\delta}{R}\right)^3 - \frac{1}{560}\left(\frac{\delta}{R}\right)^4 \right] \tag{56}$$

so that the third term in the momentum equation becomes

$$\left[\frac{V^2}{B^2}\right]\left[\frac{C}{R}\right]\frac{d\delta}{dx} + G\left[-\frac{2V^2}{R}\frac{A}{B^3}\right]\frac{d\delta}{dx}$$

or

$$\frac{d\delta}{dx}\left[\frac{V^2}{R}\right]\left[\frac{C}{B^2} - \frac{2GA}{B^3}\right] \tag{57}$$

The fourth term of (40) is then considered,

$$\frac{d}{dx}\left[\left\{1 - 2\left(\frac{\delta}{R}\right) + \left(\frac{\delta}{R}\right)^2\right\}U^2\right] \tag{58}$$

Carrying out the differentiation, we have

$$\left[1 - 2\left(\frac{\delta}{R}\right) + \left(\frac{\delta}{R}\right)^2\right]2U\frac{dU}{dx} + \frac{U^2}{R}\left[-2 + 2\left(\frac{\delta}{R}\right)\right]\frac{d\delta}{dx} \tag{59}$$

Substituting into this the values for U and dU/dx from continuity results in

$$\left[1 - 2\left(\frac{\delta}{R}\right) + \left(\frac{\delta}{R}\right)^2\right]\left[-\frac{2V^2}{R}\frac{A}{B^3}\right]\frac{d\delta}{dx} + \frac{V^2}{R}\left[\frac{1}{B^2}\right]\left[-2 + 2\left(\frac{\delta}{R}\right)\right]\frac{d\delta}{dx} \tag{60}$$

Now, setting

$$\mathcal{D} \equiv \left[1 - 2\left(\frac{\delta}{R}\right) + \left(\frac{\delta}{R}\right)^2\right] \quad ; \quad F \equiv \left[-2 + 2\left(\frac{\delta}{R}\right)\right] \tag{61},(62)$$

this term becomes

$$\frac{d\delta}{dx}\left[\frac{V^2}{R}\right]\left[-\frac{2A\mathcal{D}}{B^3} + \frac{F}{B^2}\right] \tag{63}$$

By equating the four terms just evaluated, the momentum equation can be written in the form,

$$-\frac{V^2}{R}\frac{A}{B^3}\frac{d\delta}{dx} - \frac{2\nu V}{R\delta}\frac{E}{B} = \frac{d\delta}{dx}\frac{V^2}{R}\left[\frac{C}{B^2} - \frac{2GA}{B^3}\right] + \frac{d\delta}{dx}\frac{V^2}{R}\left[-\frac{2A\mathcal{D}}{B^3} + \frac{F}{B^2}\right] \tag{64}$$

Rearranging, and letting $Re_D = VD/\nu$,

$$-\frac{4}{Re_D} = \frac{d\delta}{dx}\left[\frac{A}{B^2} + \frac{C}{B} - \frac{2GA}{B^2} - \frac{2A\mathcal{D}}{B^2} + \frac{F}{B}\right]\left[\frac{\delta}{R}\right]\frac{1}{E} \tag{65}$$

Now let

$$\mathcal{F}\left(\frac{\delta}{R}\right) \equiv \left[\frac{A}{B^2} + \frac{C}{B} - \frac{2GA}{B^2} - \frac{2A\mathcal{D}}{B^2} + \frac{F}{B}\right]\left[\frac{\delta}{R}\right]\frac{1}{E} \tag{66}$$

so that we obtain

$$-\frac{4}{Re_D} = \mathcal{F}\left(\frac{\delta}{R}\right)\frac{d\delta}{dx} \tag{67}$$

Separating variables, we may now integrate the expression

$$\int_0^{\delta/R} \mathcal{F}\left(\frac{\delta}{R}\right) d\left(\frac{\delta}{R}\right) = -8\frac{Re_x}{Re_D^2} \tag{68}$$

and find Re_x/Re_D^2 as a function of (δ/R). This has been done graphically by calculating $\mathcal{F}\left(\frac{\delta}{R}\right)$ at several values of (δ/R). A curve of $\mathcal{F}$ vs. (δ/R) is then plotted, and the area under the curve up to any (δ/R) is the value of $-8Re_x/Re_D^2$ at that (δ/R). Also, from continuity (43), we may find the value of U/V at that (δ/R). Then from Eq. (24), Appendix C, we have

$$4\bar{f}_{APP}\frac{x}{D} = \left(\frac{U}{V}\right)^2 - 1 \tag{69}$$

Thus a value of $4\bar{f}_{APP}(x/D)$ is obtained at each value of Re_x/Re_D^2, and a curve may be plotted which is shown in Figure 31. Numerical values obtained during the graphical evaluation are tabulated in Table III.

Verification of the Fifth Boundary Condition

We shall now return to the last boundary condition and give a verification that the constant a_2 is equal to zero as previously stated. The boundary condition to be fulfilled was that at $y = 0$:

$$\frac{\partial^2 u}{\partial y^2} + \frac{1}{y-R}\frac{\partial u}{\partial y} = -\frac{U}{\nu}\frac{dU}{dx} \tag{31}$$

Substituting

$$\left[\frac{\partial^2 u}{\partial y^2}\right]_{y=0} = \frac{U}{\delta^2}\left[-2\left(\frac{\delta}{R}\right)\right] \tag{70}$$

TABLE III

Summary of Factors Obtained in Graphical Integration

(δ/R)	A	B	C	$\mathcal{D}$	E	F	G
0	-.75000	1.00000	0.97143	1.00000	1.50000	-2.00000	0
0.005	-.74717	0.99625	0.96546	0.99003	1.50250	-1.99000	.00484
0.010	-.74434	0.99253	0.95948	0.98010	1.50500	-1.98000	.00965
0.050	-.72192	0.96320	0.91143	0.90250	1.52500	-1.90000	.04707
0.100	-.69433	0.92780	0.85084	0.81000	1.55000	-1.80000	.09114
0.300	-.58900	0.79960	0.60242	0.49000	1.65000	-1.40000	.23662
0.500	-.49167	0.69163	0.34405	0.25000	1.75000	-1.00000	.33143
0.600	-.44600	0.64480	0.21103	0.16000	1.80000	-0.80000	.35921
0.800	-.36067	0.56427	-.06290	0.04000	1.90000	-0.40000	.37420
1.000	-.28333	0.50000	-.34762	0	2.00000	0	.33333

(δ/R)	$\mathcal{F}$
0	0
0.005	-.00094
0.010	-.00192
0.050	-.01071
0.100	-.02425
0.300	-.10544
0.500	-.22315
0.600	-.29073
0.800	-.42721
1.000	-.53651

(δ/R)	$Re_x/Re_D{}^2$	$4\mathcal{F}_{APP}(x/D)$
0.050	0.0000318	0.07786
0.100	0.000135	0.16169
0.200	0.000638	0.34874
0.300	0.00164	0.56406
0.400	0.00328	0.81046
0.500	0.00566	1.09049
0.600	0.00887	1.40519
0.700	0.01299	1.75569
0.800	0.01794	2.14073
0.900	0.02364	2.55730
1.000	0.03002	3.00000

$$\left[\frac{\partial u}{\partial y}\right]_{y=0} = \frac{U}{\delta}\left[\frac{3}{2} + \frac{1}{2}\left(\frac{\delta}{R}\right)\right] \tag{71}$$

we have,

$$\frac{U}{\delta^2}\left[-2\left(\frac{\delta}{R}\right)\right] - \frac{U}{\delta R}\left[\frac{3}{2} + \frac{1}{2}\left(\frac{\delta}{R}\right)\right] = -\frac{U}{\nu}\frac{dU}{dx} \tag{72}$$

Substituting

$$\frac{dU}{dx} = -\frac{V}{R}\left[\frac{A}{B^2}\right]\frac{d\delta}{dx}$$

we obtain,

$$-2\left(\frac{\delta}{R}\right) - \frac{3}{2}\left(\frac{\delta}{R}\right) - \frac{1}{2}\left(\frac{\delta}{R}\right)^2 = Re_\delta \frac{d\delta}{dx}\frac{A}{B^2}\left(\frac{\delta}{R}\right) \tag{73}$$

$$\text{where } Re_\delta = V\delta/\nu$$

But,

$$\frac{d\delta}{dx} = -\frac{4}{Re_D}\frac{1}{\mathcal{F}} = -\frac{4}{Re_D}\frac{1}{\left[\frac{A}{B^2} + \frac{C}{B} - \frac{2GA}{B^2} - \frac{2A\mathcal{D}}{B^2} + \frac{F}{B}\right]\left[\frac{\delta}{R}\right]\frac{1}{E}}$$

Then (73) reduces to,

$$\frac{7}{4}\left(\frac{\delta}{R}\right) + \frac{1}{4}\left(\frac{\delta}{R}\right)^2 = \left(\frac{\delta}{R}\right)\frac{EA}{\left[A + CB - 2GA - 2A\mathcal{D} + FB\right]} \tag{74}$$

If a_2 had not been equal to zero there would be a constant term on the left hand side of (74). However, there are no constant terms on the right hand side as the first term will be of order (δ/R). Thus to partially satisfy the relation (74), a_2 had to equal zero as stated previously.

Continuation of Curve of $4\bar{f}_{APP}(x/D)$ vs. $Re_x/Re_D{}^2$

On Figure 31 the boundary layers meet when $4\bar{f}_{APP}(x/D)$ is exactly equal to three, at which point $(x/D) = 0.03002 \, Re_D$ (the latter value is a little larger than the value, $(x/D) = 0.02875 \, Re_D$, which was obtained by Schiller[16]). Beyond the point where $(\delta/R) = 1$ we may extend the curve by using the Hagen-Poiseuille Law. Thus we write,

$$\Delta 4\bar{f}_{APP}\frac{x}{D} = \frac{\Delta p}{\frac{1}{2}\rho V^2} = 4f_{HAGEN-POISEUILLE}\frac{\Delta x}{D} = \frac{64}{Re_D}\frac{\Delta Re_x}{Re_D} = 64\Delta\left(\frac{Re_x}{Re_D{}^2}\right) \tag{75}$$

where Δ signifies that this is the additional friction factor to be added to $4\bar{f}_{APP}(x/D) = 3$. Thus for example when $\Delta Re_x/Re_D^2 = 0.07$; $\Delta 4\bar{f}_{APP}(x/D) = 64(0.07) = 4.48$. Then $4\bar{f}_{APP}(x/D) = 3 + \Delta 4\bar{f}_{APP}(x/D) = 3 + 4.48 = 7.48$. Thus a point is plotted at $Re_x/Re_D^2 = 0.07 + 0.03 = 0.10$ and $4\bar{f}_{APP}(x/D) = 7.48$, through which the curve may be extended. The theoretical curve obtained (Figure 31) follows the data of Kline and Shapiro[6] for the beginning of the entry region, and then gradually approaches the Hagen-Poiseuille line.

Behavior of the Solution as (δ/R) Approaches Zero

To determine how the solution behaves in the region very close to the entry of the tube as (δ/R) goes to zero, we begin with expression (66) and neglect terms of order higher than (δ/R). This results in,

$$\mathcal{F}\left(\frac{\delta}{R}\right) \cong \frac{1}{\left[\frac{3}{2} + \frac{1}{2}\left(\frac{\delta}{R}\right)\right]} \left\{ \frac{\left[-\frac{3}{4} + \frac{17}{30}\left(\frac{\delta}{R}\right) + \frac{102}{70}\left(\frac{\delta}{R}\right) + \frac{3}{2} - \frac{42}{15}\left(\frac{\delta}{R}\right)\right]}{\left[1 - \frac{3}{4}\left(\frac{\delta}{R}\right)\right]^2} \right.$$
$$\left. + \frac{\left[\frac{34}{35} - \frac{1003}{840}\left(\frac{\delta}{R}\right) - 2 + 2\left(\frac{\delta}{R}\right)\right]}{\left[1 - \frac{3}{4}\left(\frac{\delta}{R}\right)\right]} \right\} \left(\frac{\delta}{R}\right)$$

$$\mathcal{F}\left(\frac{\delta}{R}\right) \cong \frac{\left[\frac{3}{4} - \frac{36}{35}\right]\left[\frac{\delta}{R}\right]}{\frac{3}{2}}$$

which reduces to,

$$\mathcal{F}\left(\frac{\delta}{R}\right) \cong -\frac{39 \times 2}{140 \times 3}\left(\frac{\delta}{R}\right) \tag{76}$$

Integrating according to (68) we have,

$$-\frac{78}{420}\int_0^{\delta/R}\left(\frac{\delta}{R}\right)d\left(\frac{\delta}{R}\right) \cong -8\frac{Re_x}{Re_D^2}$$

which becomes,

$$\frac{Re_x}{Re_D^2} \cong \frac{13}{1120}\left(\frac{\delta}{R}\right)^2 \tag{77}$$

Thus,

$$\left(\frac{\delta}{R}\right) \cong 9.29 \frac{\sqrt{Re_x}}{Re_D} \qquad \text{as } \left(\frac{\delta}{R}\right) \longrightarrow 0 \qquad (73)$$

From continuity (43) we obtain,

$$\frac{U}{V} = \frac{1}{\left[1 - \frac{3}{4}\left(\frac{\delta}{R}\right) + \cdots\right]} = 1 + \frac{3}{4}\left[9.29 \frac{\sqrt{Re_x}}{Re_D}\right] + \cdots$$

$$\frac{U}{V} = 1 + 6.96 \frac{\sqrt{Re_x}}{Re_D} + \cdots \qquad (79)$$

Then we have,

$$4\bar{f}_{APP} \frac{x}{D} = \left(\frac{U}{V}\right)^2 - 1 \cong 13.92 \frac{\sqrt{Re_x}}{Re_D} \qquad (80)$$

which is valid near the pipe entry. This is shown as a dashed line on Figure 31, and may be compared with the experimental value $13.74\sqrt{Re_x}/Re_D$ of Kline and Shapiro[6].

As a check on this result, we have for the flat plate profile $u/U = \frac{3}{2}\left(\frac{y}{\delta}\right) - \frac{1}{2}\left(\frac{y}{\delta}\right)^3$ (see reference 18, pages 190-191),

$$\delta(x) = \sqrt{\frac{2\beta_1}{\alpha_1}}\sqrt{\frac{\nu x}{U_\infty}} = \sqrt{\frac{2 \times \frac{3}{2}}{\frac{39}{280}}}\sqrt{\frac{\nu x}{U_\infty}} = \sqrt{\frac{280}{13}}\sqrt{\frac{\nu x}{U_\infty}}$$

$$\frac{\delta}{R} = \sqrt{\frac{1120}{13}}\left[\frac{U_\infty x/\nu}{U_\infty^2 D^2/\nu^2}\right]^{1/2} = 9.29 \frac{\sqrt{Re_x}}{Re_D} \qquad (81)$$

which is equivalent to (78).

Local Apparent Friction Factor Along the Tube

The method developed has led directly to an expression for the mean apparent friction factor $\bar{f}_{APP}$, but it is also of interest to observe the variation in the local apparent friction factor, f_{APP}, along the tube. This can be found by differentiating the log-log plot for mean apparent friction factor in the following manner. Beginning with the definition for mean apparent friction factor we have,

$$4\bar{f}_{APP} = \frac{1}{(x/D)}\int_0^{x/D} 4f_{APP} \, d\left(\frac{x}{D}\right) \qquad (82)$$

Differentiating results in,

$$4f_{APP} = \frac{d}{d(^x/_D)}\left[4\bar{f}_{APP}\left(\frac{X}{D}\right)\right]$$

which is equivalent to,

$$4f_{APP}\,Re_D = \frac{d}{d\left(\frac{Re_x}{Re_D^2}\right)}\left[4\bar{f}_{APP}\,\frac{X}{D}\right] = \frac{\frac{1}{4\bar{f}_{APP}\frac{X}{D}}\,d\left(4\bar{f}_{APP}\frac{X}{D}\right)}{\frac{1}{Re_x/Re_D^2}\,d\left(Re_x/Re_D^2\right)}\cdot\frac{4\bar{f}_{APP}\,\frac{X}{D}}{Re_x/Re_D^2}$$

Finally we have,

$$4f_{APP}\,Re_D = \left[\frac{Re_D^2}{Re_x}\right]\left[\frac{d\left(\ln 4\bar{f}_{APP}\,\frac{X}{D}\right)}{d\left(\ln Re_x/Re_D^2\right)}\right]4\bar{f}_{APP}\,\frac{X}{D} \tag{33}$$

By measuring the slope of the mean apparent friction factor curve (Figure 31), it is possible to determine values of the parameter $4f_{APP}Re_D$ at various values of Re_x/Re_D^2. The universal curve thus obtained is shown in Figure 32, and is in agreement with the experimental data of Kline and Shapiro[6] (the experimental data extend up to $Re_x/Re_D^2 = 10^{-3}$).

These results can also be plotted as $4f_{APP}$ vs. Re_x. In this case a family of curves is obtained (Figure 33), each curve being for a different diameter Reynolds number.

Growth of the Laminar Boundary Layer Within a Tube Entry

The values of (δ/R) vs. Re_x/Re_D^2 which were obtained from the graphical integration process have been plotted in Figure 34. The curve illustrates the manner in which the boundary layer thickness increases along the length of the tube. For comparison purposes the flat plate relation (31) has also been plotted on the same figure. The curves illustrate that the favorable pressure gradient, which is present as the flow develops within a tube entry, causes the boundary layer to grow at a decreased rate as compared with the growth on a flat plate with no external pressure gradient.

Substitution of the Pohlhausen Profile for the Cubic Profile

It is recalled that as (δ/R) approaches zero, the expression (42) reduces to a cubic flat-plate velocity profile. It was thought that a

better approximation might be obtained if the fourth order Pohlhausen profile were substituted for the cubic expression. Thus a new profile was formulated,

$$\frac{u}{U} = \left\{ \left[2\left(\frac{y}{\delta}\right) - 2\left(\frac{y}{\delta}\right)^3 + \left(\frac{y}{\delta}\right)^4 \right]\left[1 - \left(\frac{\delta}{R}\right) \right] + \left[2\left(\frac{y}{\delta}\right) - \left(\frac{y}{\delta}\right)^2 \right]\left[\frac{\delta}{R} \right] \right\} \tag{84}$$

This expression was used to evaluate the terms in the continuity and momentum equations in a manner similar to the computations previously carried out. Substitution into continuity yielded the expression,

$$U = \frac{V}{P} \tag{85}$$

where,

$$P = \left[1 - \frac{3}{5}\left(\frac{\delta}{R}\right) + \frac{1}{15}\left(\frac{\delta}{R}\right)^2 + \frac{1}{30}\left(\frac{\delta}{R}\right)^3 \right] \tag{86}$$

Differentiating with respect to x gave,

$$\frac{dU}{dx} = -\frac{V}{R}\frac{Q}{P^2}\frac{d\delta}{dx} \tag{87}$$

where,

$$Q = \left[-\frac{3}{5} + \frac{2}{15}\left(\frac{\delta}{R}\right) + \frac{1}{10}\left(\frac{\delta}{R}\right)^2 \right] \tag{88}$$

The first term in the momentum equation then became,

$$U\frac{dU}{dx} = -\frac{V^2}{R}\frac{Q}{P^3}\frac{d\delta}{dx} \tag{89}$$

The second term in the momentum equation could be immediately evaluated as

$$-\frac{2\nu}{R}\left(\frac{\partial u}{\partial y}\right)_{y=0} = -\frac{4\nu}{R\delta}\frac{V}{P} \tag{90}$$

After evaluation of the integral, the third term in the momentum equation assumed the form,

$$\frac{2}{R^2}\frac{d}{dx}\left[U^2\int_0^\delta \left(\frac{u}{U}\right)^2 (R-y)\,dy \right] = \frac{d\delta}{dx}\left[\frac{V^2}{R}\right]\left[\frac{T}{P^2} - \frac{2SQ}{P^3}\right] \tag{91}$$

where

$$S = \left[\frac{367}{315}\left(\frac{\delta}{R}\right) - \frac{280}{315}\left(\frac{\delta}{R}\right)^2 + \frac{37}{630}\left(\frac{\delta}{R}\right)^3 - \frac{1}{630}\left(\frac{\delta}{R}\right)^4 \right] \tag{92}$$

$$T = \left[\frac{367}{315} - \frac{112}{63}\left(\frac{\delta}{R}\right) + \frac{37}{210}\left(\frac{\delta}{R}\right)^2 - \frac{2}{315}\left(\frac{\delta}{R}\right)^3 \right] \tag{93}$$

Finally, the fourth term in the momentum equation became,

$$\frac{d}{dx}\left[\left\{ 1 - 2\left(\frac{\delta}{R}\right) - \left(\frac{\delta}{R}\right)^2 \right\} U^2\right] = \frac{d\delta}{dx}\left[\frac{V^2}{R}\right]\left[-\frac{2Q\mathcal{S}}{P^3} + \frac{F}{P^2} \right] \tag{94}$$

Equating the terms and simplifying yields the momentum equation in the

form,

$$-\frac{8}{Re_D} = \frac{d\delta}{dx}\left[\frac{Q}{P^2} + \frac{T}{P} - \frac{2SQ}{P^2} - \frac{2Q\mathcal{S}}{P^2} + \frac{F}{P}\right]\left[\frac{\delta}{R}\right] \tag{95}$$

Setting

$$Z\left(\frac{\delta}{R}\right) \equiv \left[\frac{Q}{P^2} + \frac{T}{P} - \frac{2SQ}{P^2} - \frac{2Q\mathcal{S}}{P^2} + \frac{F}{P}\right]\left[\frac{\delta}{R}\right] \tag{96}$$

produces the equation,

$$-\frac{8}{Re_D} = \frac{d\delta}{dx} Z\left(\frac{\delta}{R}\right) \tag{97}$$

This expression can then be integrated,

$$-16 \frac{Re_x}{Re_D^2} \int_0^{\delta/R} Z\left(\frac{\delta}{R}\right) d\left(\frac{\delta}{R}\right) \tag{98}$$

This has been carried out graphically as in the previous computation, and
the principal results are shown in Table IV. The results were found to
lie on the same curve (Figure 31) which was obtained using expression (41),
except that the entrance length was slightly smaller, the value being
x/D = 0.02961 Re$_D$, as compared with the earlier value, 0.03002 Re$_D$.

To determine the behavior of this solution as (δ/R) approaches zero,
we follow the same procedure that was used to evaluate expression (78)
with the result in this case,

$$\left(\frac{\delta}{R}\right) \cong 11.68 \frac{\sqrt{Re_x}}{Re_D} \qquad \text{as} \qquad \left(\frac{\delta}{R}\right) \longrightarrow 0 \tag{99}$$

From continuity (85) and (86) we obtain,

$$\frac{U}{V} = \frac{1}{\left[1 - \frac{3}{5}\left(\frac{\delta}{R}\right) + \cdots\right]} = 1 + \frac{3}{5}\left[11.68 \frac{\sqrt{Re_x}}{Re_D}\right] + \cdots$$

$$\frac{U}{V} = 1 + 7.01 \frac{\sqrt{Re_x}}{Re_D} + \cdots$$

TABLE IV

Summary of Factors Obtained in Graphical Integration

(δ/R)	P	Q	S	T	Z
0	1.00000	-.60000	0	1.16508	0
0.005	0.99700	-.59933	0.00580	1.15619	-0.00119
0.010	0.99401	-.59866	0.01156	1.14732	-0.00242
0.050	0.97017	-.59308	0.05604	1.07663	-0.01354
0.100	0.94070	-.58567	0.10768	0.98906	-0.03092
0.300	0.82690	-.55100	0.27110	0.64743	-0.14679
0.500	0.72083	-.50833	0.36756	0.31944	-0.35705
0.600	0.67120	-.48400	0.39153	0.16047	-0.50526
0.800	0.57973	-.42933	0.39259	-.14763	-0.89555
1.000	0.50000	-.36667	0.33333	-.44286	-1.37460

(δ/R)	Re_x/Re_D^2	$4\bar{f}_{APP}(x/D)$
0.050	0.000020	0.06244
0.100	0.000089	0.13005
0.200	0.000422	0.28276
0.300	0.00111	0.46249
0.400	0.00230	0.67442
0.500	0.00414	0.92455
0.600	0.00682	1.21971
0.700	0.01052	1.56739
0.800	0.01533	1.97539
0.900	0.02172	2.45105
1.000	0.02961	3.00000

Then we have,

$$4\bar{f}_{APP}\,\frac{x}{D} - \left(\frac{U}{V}\right)^2 - 1 \cong 14.02\,\frac{\sqrt{Re_x}}{Re_D} \tag{100}$$

as compared with the value $13.92\sqrt{Re_x}/Re_D$ obtained in the earlier calculations (Eq. (80)). Equation (99) may be checked by the use of the constants listed in reference 18 (pages 190-191), for the flat plate profile, $u/U = 2\left(\frac{y}{\delta}\right) - 2\left(\frac{y}{\delta}\right)^3 + \left(\frac{y}{\delta}\right)^4$. Thus we have,

$$\delta(x) = \sqrt{\frac{2\beta_1}{\alpha_1}}\sqrt{\frac{\nu x}{U_\infty}} \approx \sqrt{\frac{2 \times 2}{\frac{37}{315}}}\sqrt{\frac{\nu x}{U_\infty}}$$

$$\left(\frac{\delta}{R}\right) = \sqrt{\frac{5040}{37}}\,\frac{\sqrt{Re_x}}{Re_D} = 11.68\,\frac{\sqrt{Re_x}}{Re_D} \tag{101}$$

The boundary layer growth for these computations is plotted as a set of dashed lines on Figure 34.

Correction Factor for a Viscometer

In a viscometer the rate of flow and pressure drop through a tube leading from a tank is measured, and from this the fluid viscosity can be determined. The calculations are based on the assumption that fully-developed Poiseuille flow exists throughout the tube. However, due to the fact that the flow is developing in the entry region of the tube, a correction factor must be applied, as the actual loss in this region will be larger than that calculated from the fully-developed laminar equations. The pressure drop equation used for these calculations is of the form,

$$\frac{\Delta p}{\frac{1}{2}\rho V^2} = 64\,\frac{Re_x}{Re_D^2} + 1 + \text{Correction Constant} \tag{102}$$

The first term on the right represents the pressure loss in the tube if fully-developed laminar flow were to exist throughout the entire tube length. The second term represents the change in kinetic energy from the tank to the tube entry, and the third term is the correction factor which must be applied. This correction factor may be easily calculated by

taking the actual total friction drop in the entry region of the tube (up to $(\delta/R) = 1$) and subtracting the friction drop that would occur in that length for fully-developed laminar flow. Thus we have for the case when velocity profile (41) was used,

$$\text{Correction} = 3.000 - 64(0.03002) = 1.079$$

For the velocity profile (84) we have,

$$\text{Correction} = 3.000 - 64(0.02961) = 1.105$$

Values for this correction have been calculated by other investigators, their results being as follows: Schiller[16], 1.16; Langhaar[7], 1.28; Boussinesq[1], 1.24; and Atkinson and Goldstein[5], 1.41. Experimental values summarized by Langhaar[7], range from 1.24 to 1.32, so it appears that the values computed by the present method may be slightly low, with the Pohlhausen type approximation (84) producing a slightly better result than the profile of equation (41). In the actual experiments there may be a frictional loss at the tube entry, which might account partially for the difference between the observed values and the present computations.
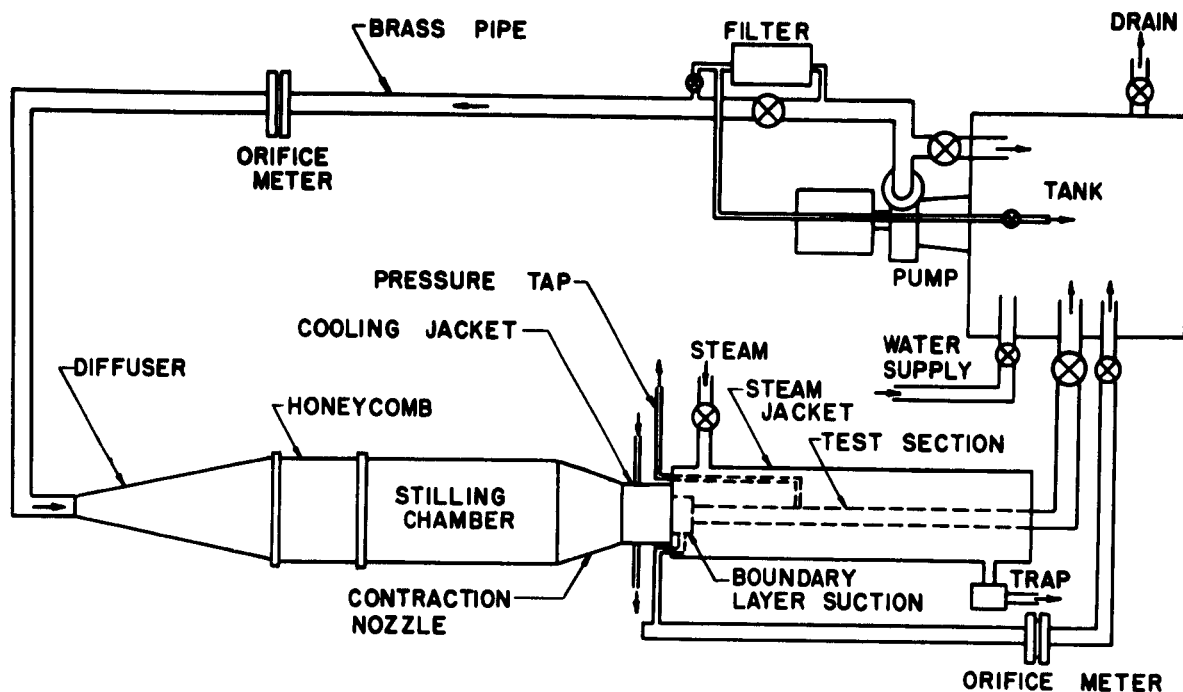
BRASS PIPE

FILTER

DRAIN

ORIFICE METER

TANK

PUMP

PRESSURE TAP

COOLING JACKET

STEAM

WATER SUPPLY

DIFFUSER

STEAM JACKET

HONEYCOMB

TEST SECTION

STILLING CHAMBER

CONTRACTION NOZZLE

BOUNDARY LAYER SUCTION

TRAP

ORIFICE METER

FIG. 1 SCHEMATIC DIAGRAM OF THE FLOW SYSTEM

ALUMINUM TUBES
0.200" O.D., 8.9" LONG
0.004" WALL

O-RING SEAL

FLOW

2"

10"

DIFFUSER

HONEYCOMB

DAMPING SCREEN
34 MESH ,
0.0065" DIAM. WIRE

FIG. 2 THE STILLING CHAMBER. THE FLOW WAS STRAIGHTENED BY A
HONEYCOMB CONSISTING OF TIGHTLY PACKED EXTRUDED ALUMINUM
TUBES. THIS WAS FOLLOWED BY 15 STAINLESS STEEL TURBULENCE
DAMPING SCREENS (2 SHOWN IN FIGURE) WHICH WERE EACH SOLDERED
TO AN INTERLOCKING   ANNULAR BRONZE RING

FIG. 3   DOUBLE CONTRACTION NOZZLES AND BOUNDARY LAYER SUCTION
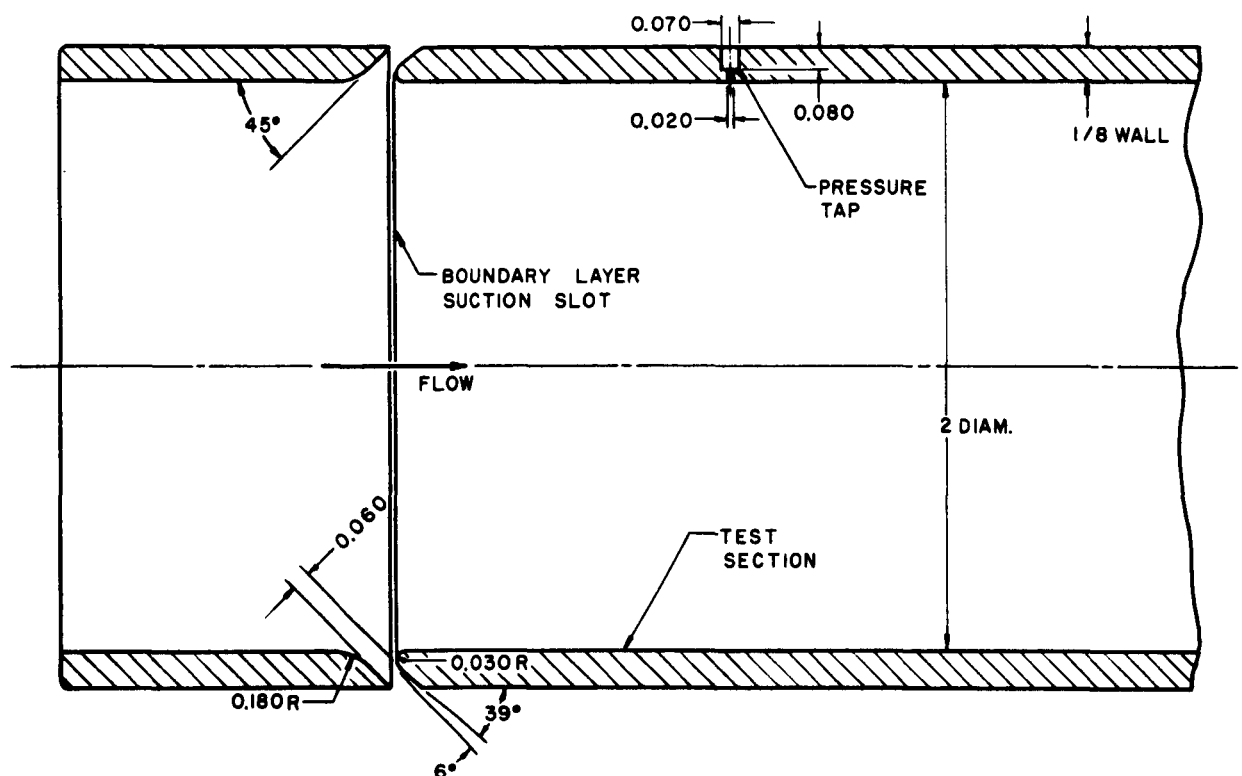AT THE TEST SECTION ENTRY.

FIG. 4   TEST SECTION ENTRY SHOWING THE CONFIGURATION OF THE
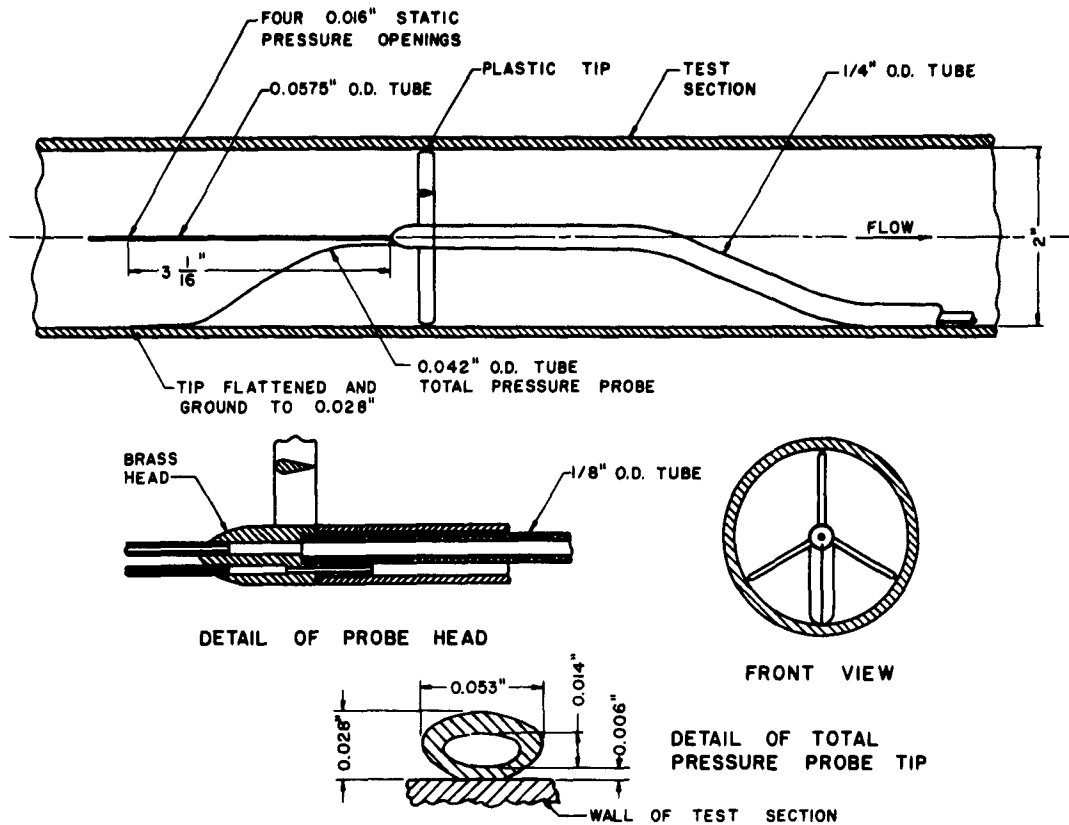BOUNDARY LAYER SUCTION SLOT AND PRESSURE TAPS.

FIG. 5 BOUNDARY LAYER PROBE. THIS WAS INSERTED THROUGH THE
EXIT END OF THE TEST SECTION. IT MEASURED THE TOTAL
PRESSURE IN THE BOUNDARY LAYER AT A FIXED DISTANCE
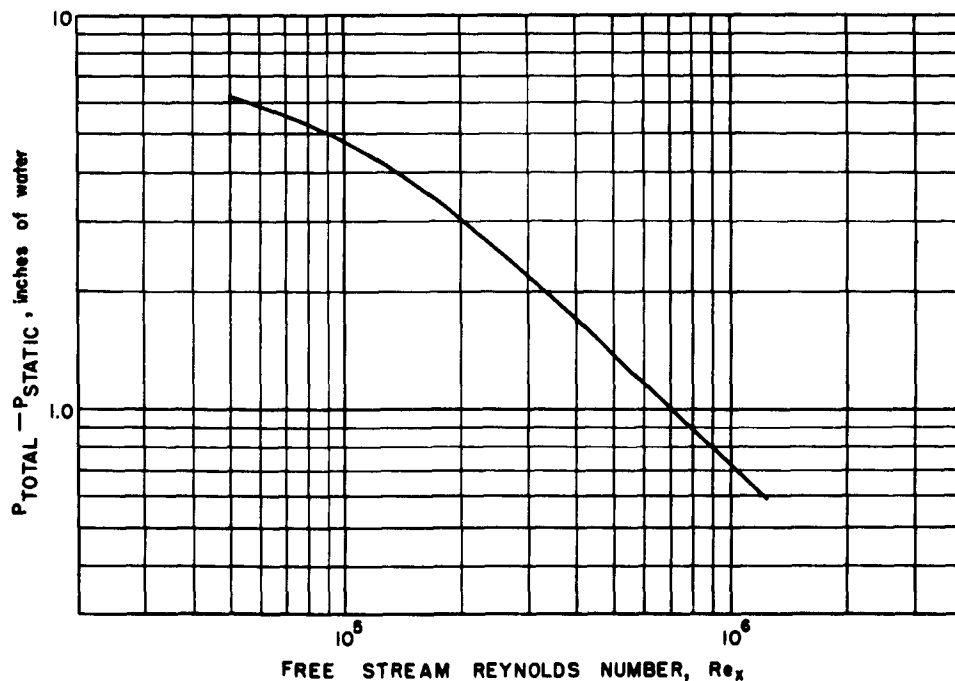FROM THE WALL, AS WELL AS THE STATIC PRESSURE IN THE
CORE OF THE FLOW.

FREE STREAM REYNOLDS NUMBER, Re_x

FIG. 6 CURVE CALCULATED FOR LAMINAR ZONE AS INDICATED IN
APPENDIX B. TOTAL PRESSURE PROBE ASSUMED FIXED
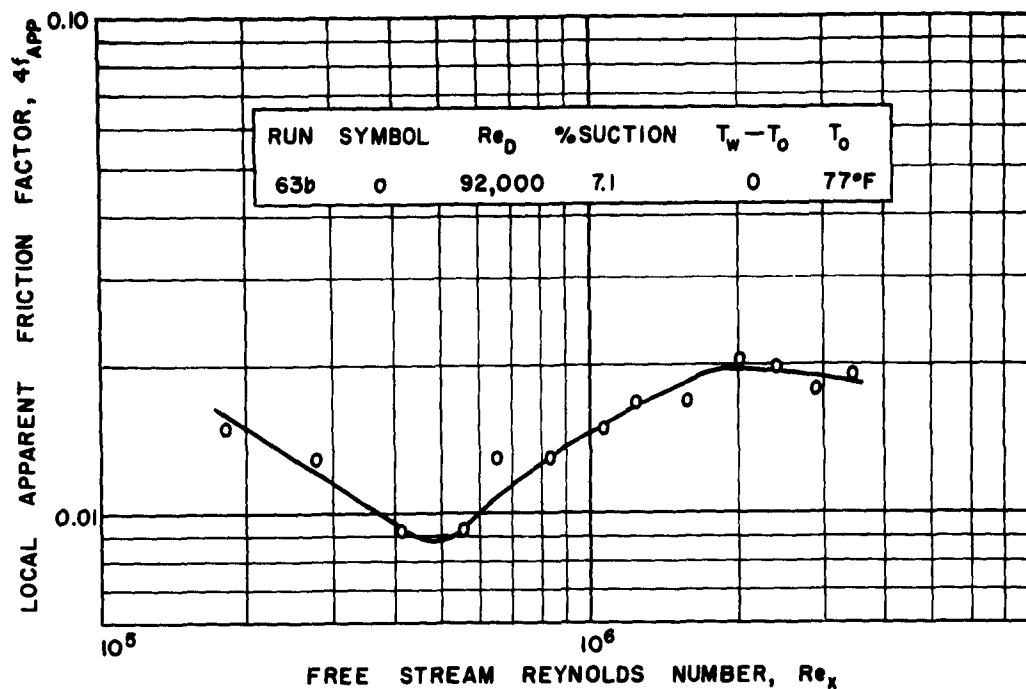0.020" FROM WALL. Re_D = 100,000 T_0 = 75°F

FIG. 7   ADIABATIC RUN WITH TRANSITION DETERMINED FROM LOCAL APPARENT FRICTION FACTOR MEASUREMENTS. TO BE COMPARED WITH FIGURE 8 SHOWING THE SAME RUN WITH TRANSITION DETERMINED BY THE BOUNDARY LAYER PROBE
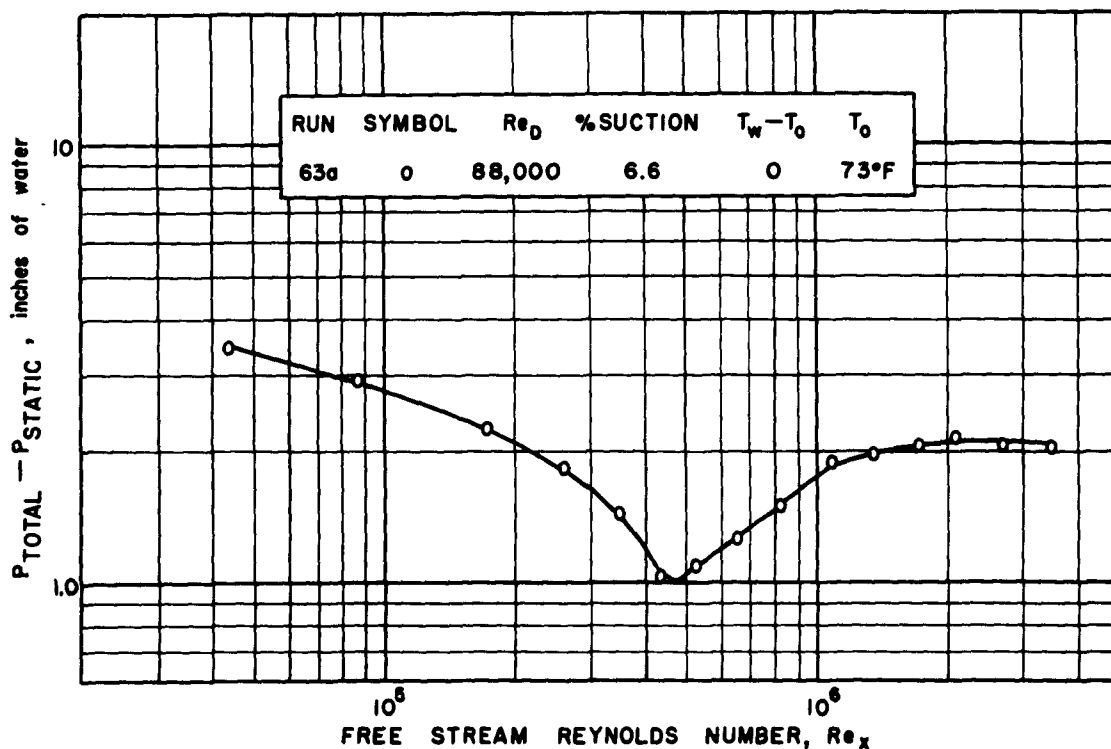

FIG. 8   SAME RUN AS IN FIG. 7. A COMPARISON OF FIGS. 7 & 8 SHOWS THAT THE BOUNDARY LAYER PROBE INDICATED TRANSITION AT THE SAME Re_x AS THE FRICTION FACTOR MEASUREMENTS.
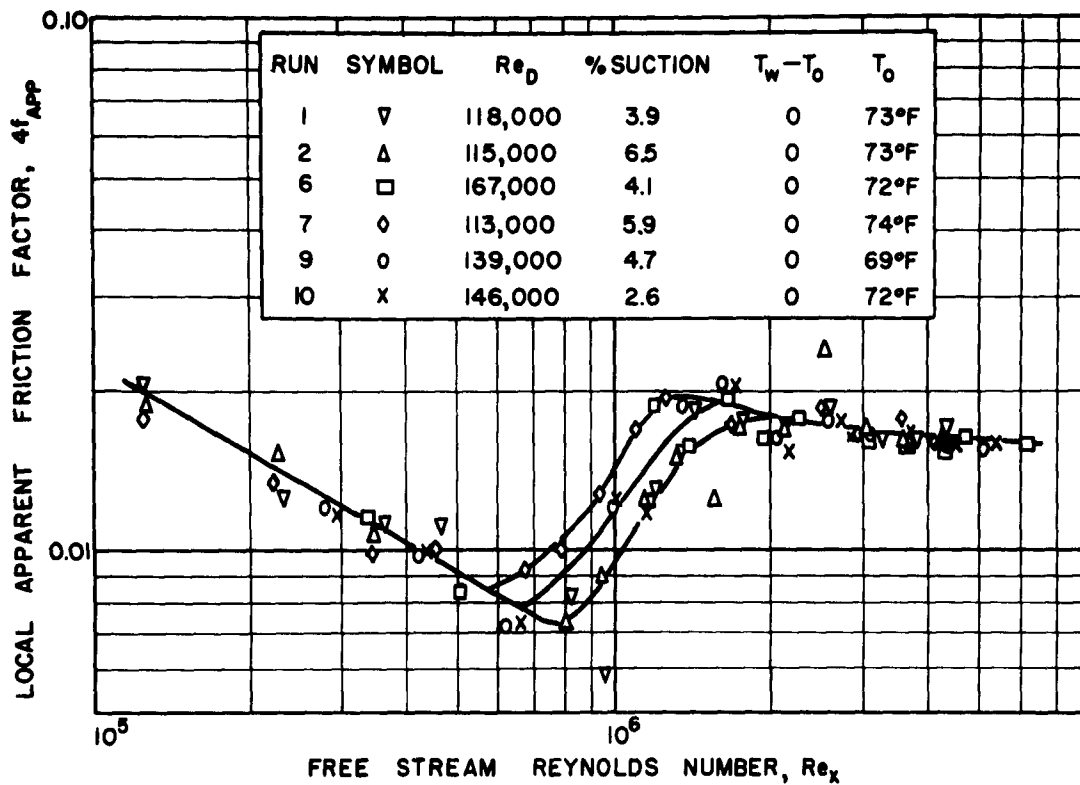
RUN	SYMBOL	Re_D	%SUCTION	$T_w - T_o$	T_o
1	▽	118,000	3.9	0	73°F
2	△	115,000	6.5	0	73°F
6	□	167,000	4.1	0	72°F
7	◇	113,000	5.9	0	74°F
9	o	139,000	4.7	0	69°F
10	X	146,000	2.6	0	72°F

FIG. 9 ADIABATIC PERFORMANCE OF THE SYSTEM FOR SEVERAL FLOW RATES AND RATES OF BOUNDARY LAYER SUCTION.

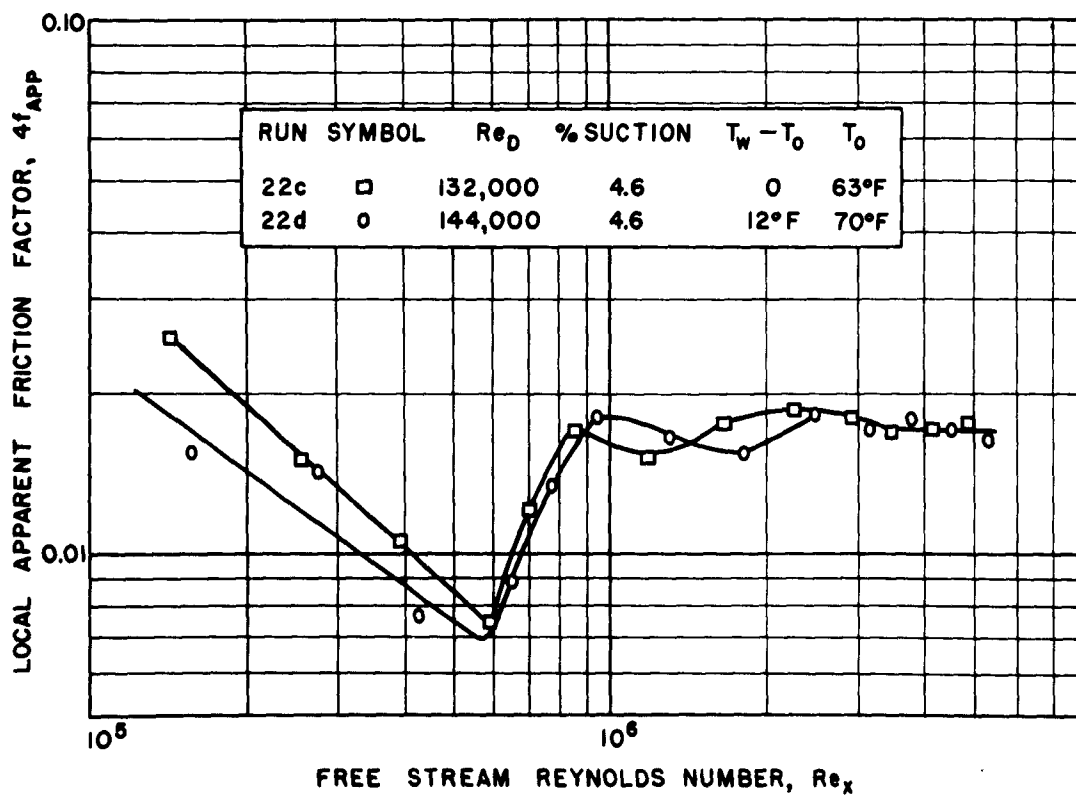| RUN	SYMBOL	Re_D	%SUCTION	$T_w - T_o$	T_o
22c	□	132,000	4.6	0	63°F
22d	o	144,000	4.6	12°F	70°F

FIG. 10 THE EFFECT OF HEATING ON TRANSITION. SMALL TEMPERATURE DIFFERENCE.
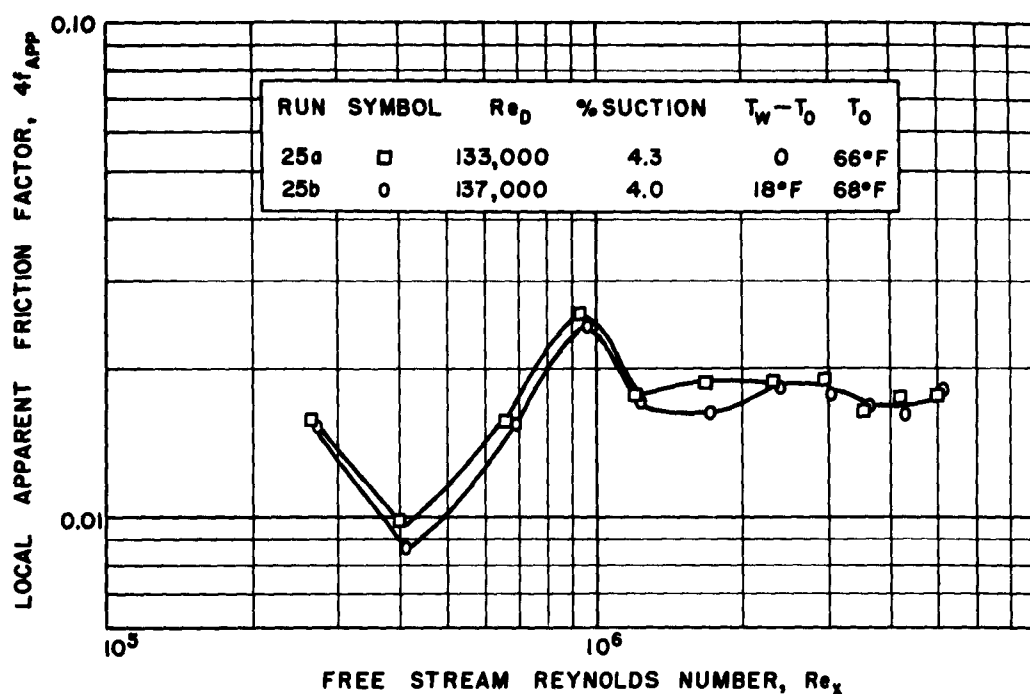
FIG. II   THE EFFECT OF HEATING ON TRANSITION.   A   COMPARISON
WITH FIG. IO   INDICATES A DECREASE IN TRANSITION Re_x
DUE TO ACCUMULATION OF DIRT PARTICLES ON WALLS.
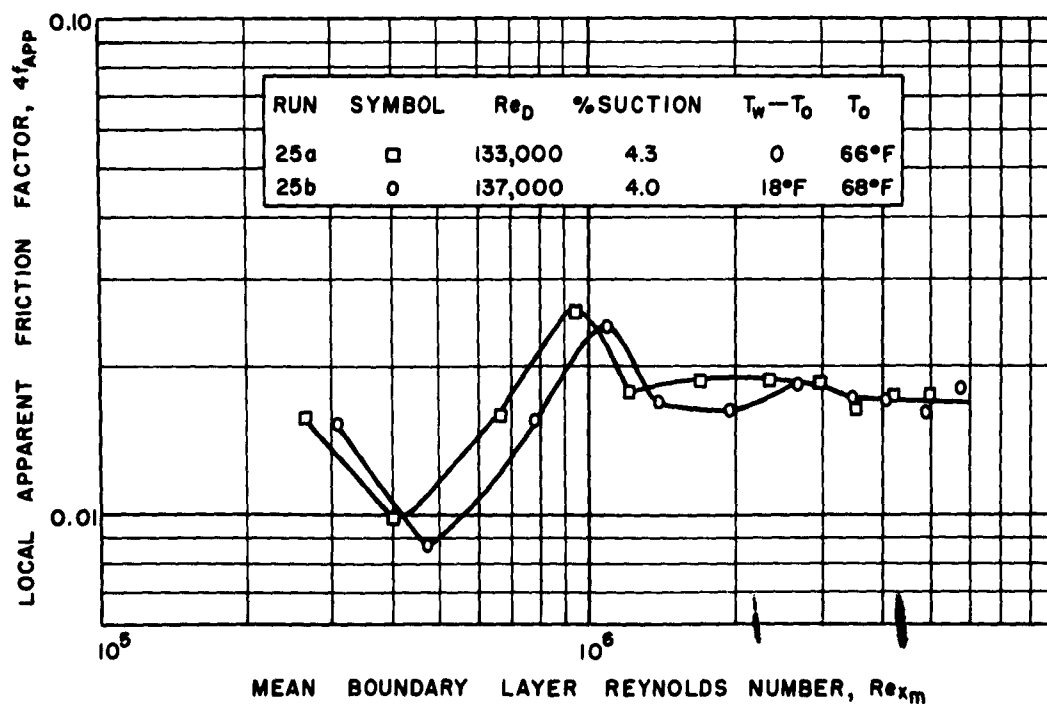

FIG. 12   THE   EFFECT   OF   HEATING   ON   TRANSITION.   SAME AS
FIG. II, EXCEPT THAT MEAN BOUNDARY LAYER REYNOLDS
NUMBER IS USED IN PLACE OF FREE STREAM
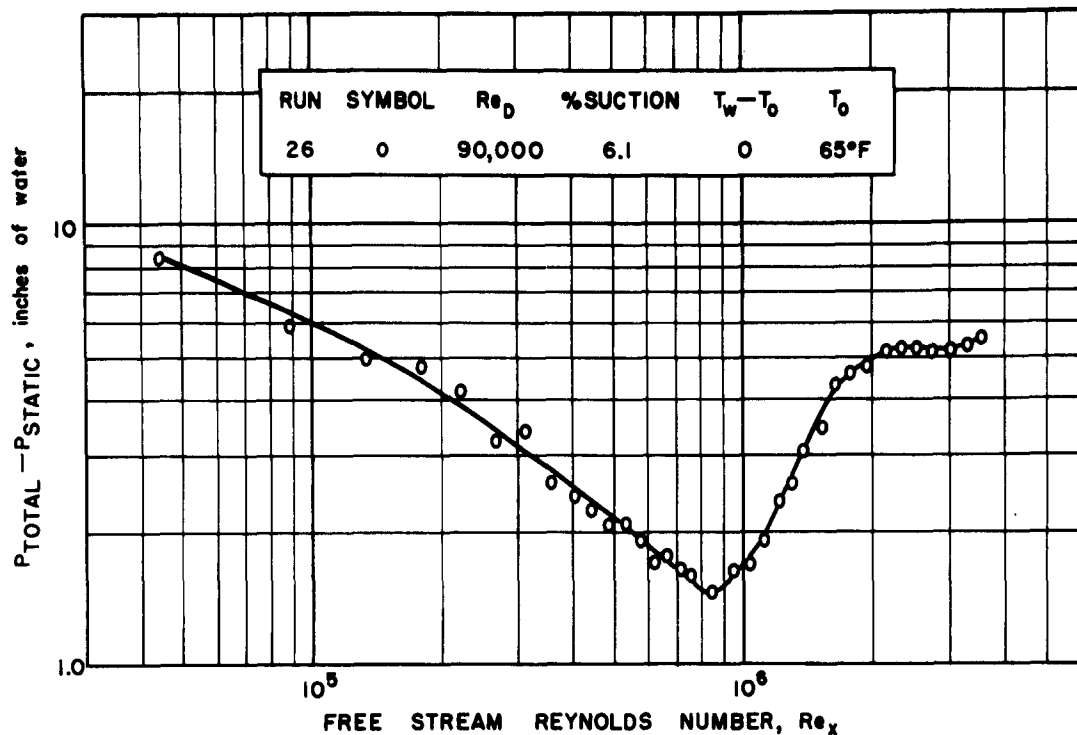REYNOLDS   NUMBER.

FIG. 13   ADIABATIC RUN USING BOUNDARY LAYER PROBE. RUN
TAKEN AFTER SYSTEM HAD JUST BEEN THOROUGHLY
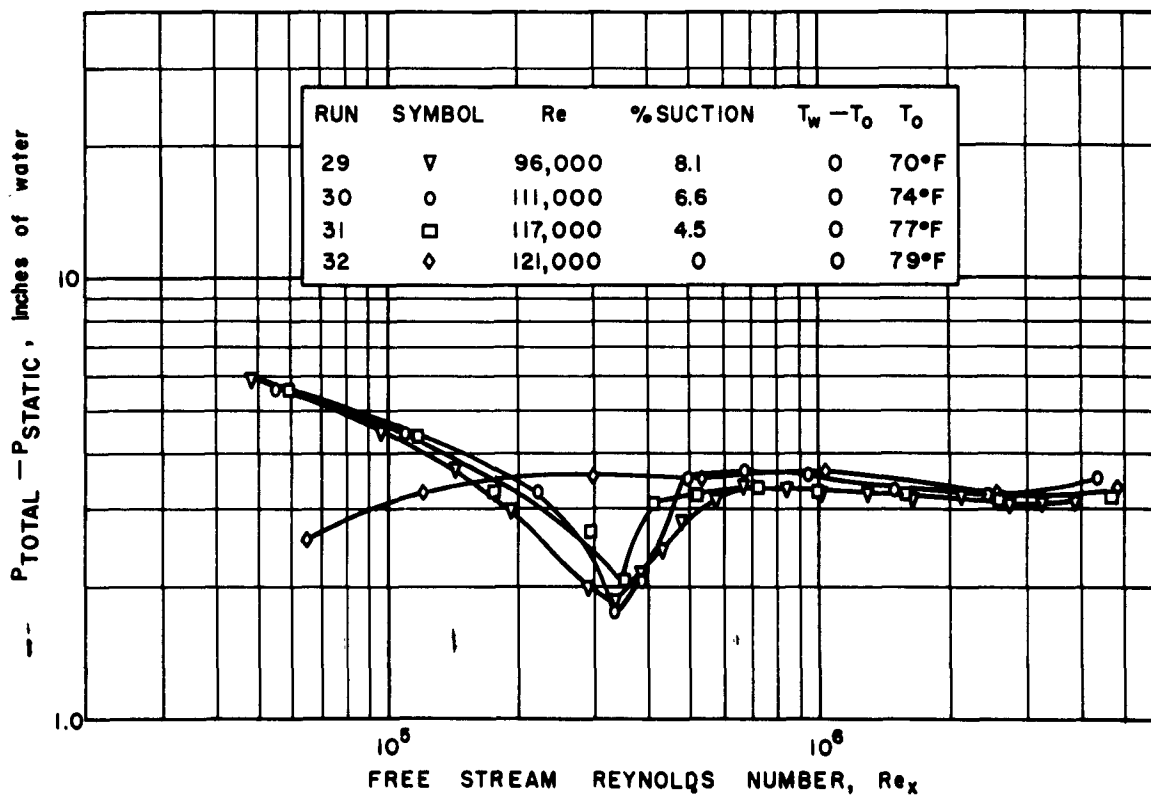CLEANED.

FIG. 14   THE EFFECT OF BOUNDARY LAYER SUCTION RATE ON
THE ADIABATIC PERFORMANCE OF THE SYSTEM.
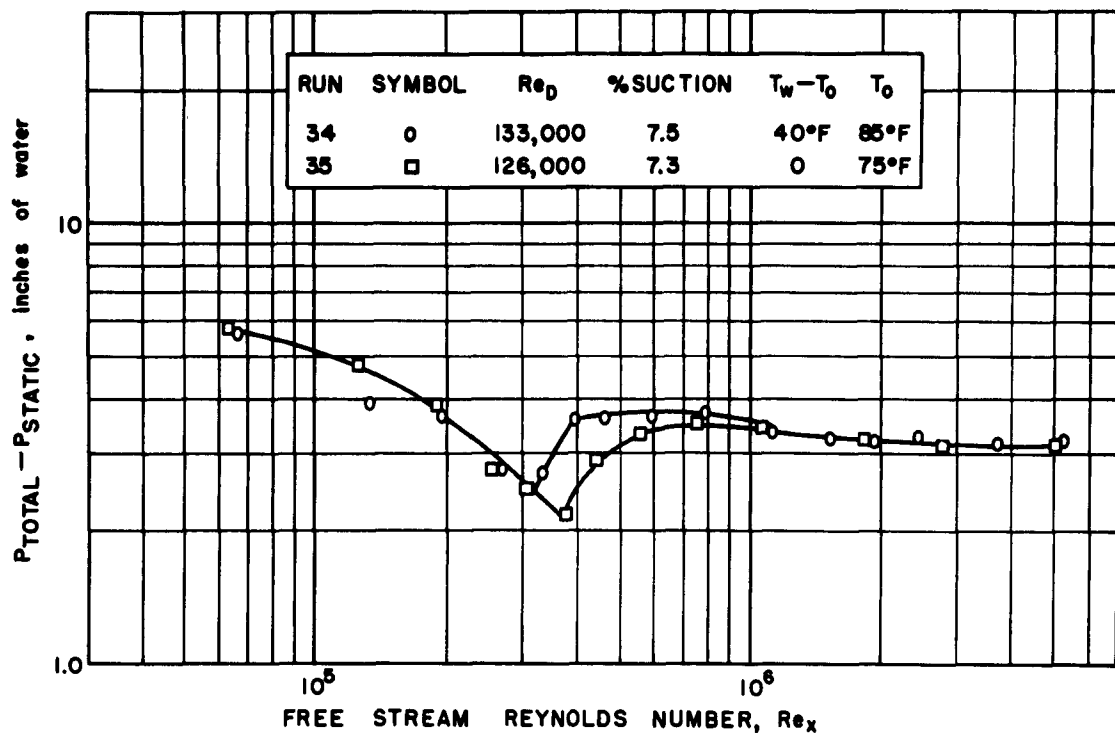
FIG. 15   THE   EFFECT   OF   HEATING   ON   TRANSITION   FOR   A   FLOW
RATE   GIVING $Re_D \cong$ 130,000.

FIG. 16   THE   EFFECT   OF   HEATING   ON   TRANSITION.   SAME   AS
FIG. 15, EXCEPT   THAT   MEAN   BOUNDARY   LAYER   REYNOLDS
NUMBER   IS   USED   IN   PLACE   OF   FREE   STREAM
REYNOLDS   NUMBER.

FIG. 17   THE EFFECT   OF   HEATING   ON   TRANSITION.   THE EFFECT
OF BOUNDARY   LAYER SUCTION RATE   ON THE   ADIABATIC
PERFORMANCE   OF   THE   SYSTEM   FOR   THE   SAME Re_D
IS ALSO   SHOWN.
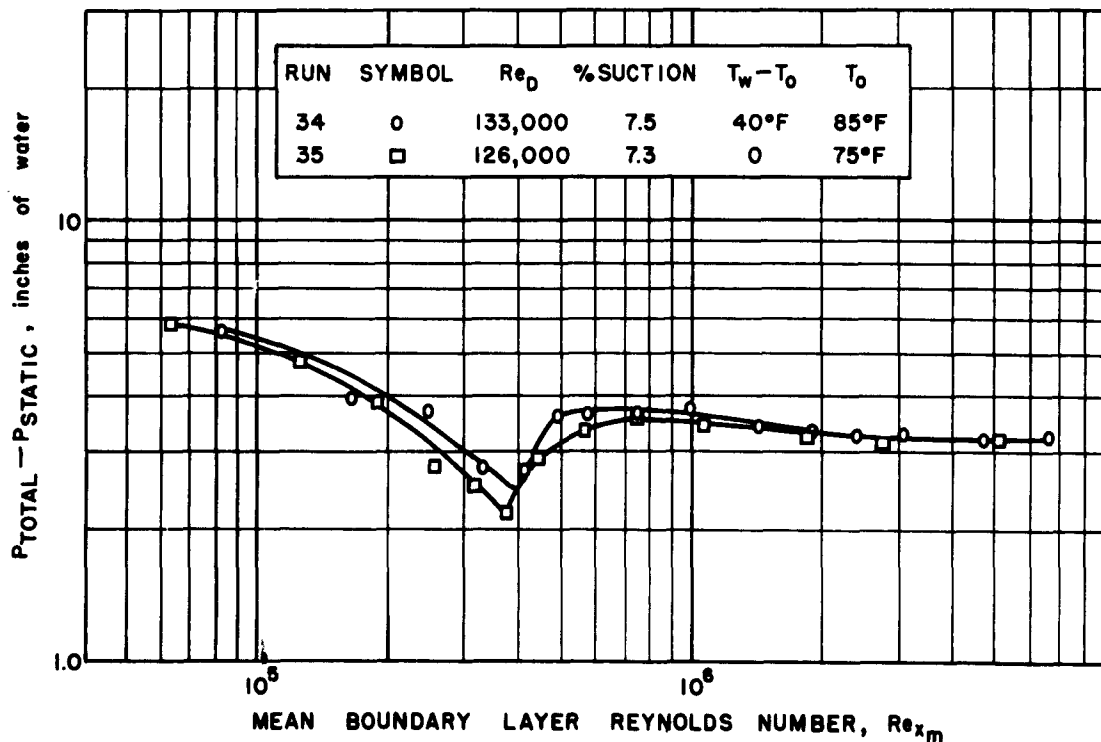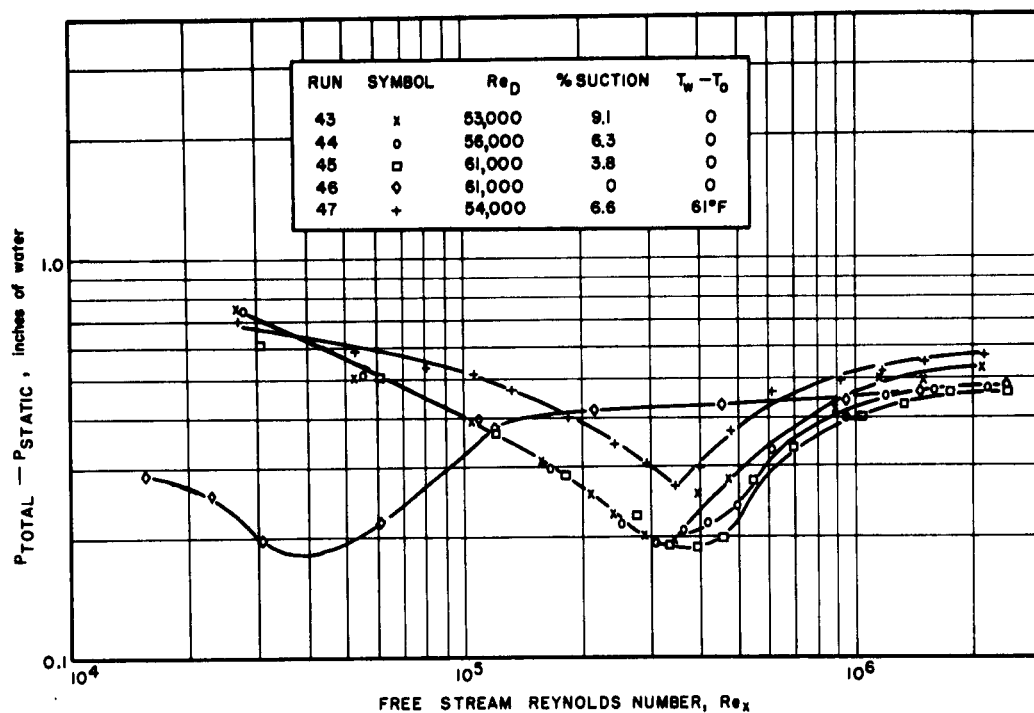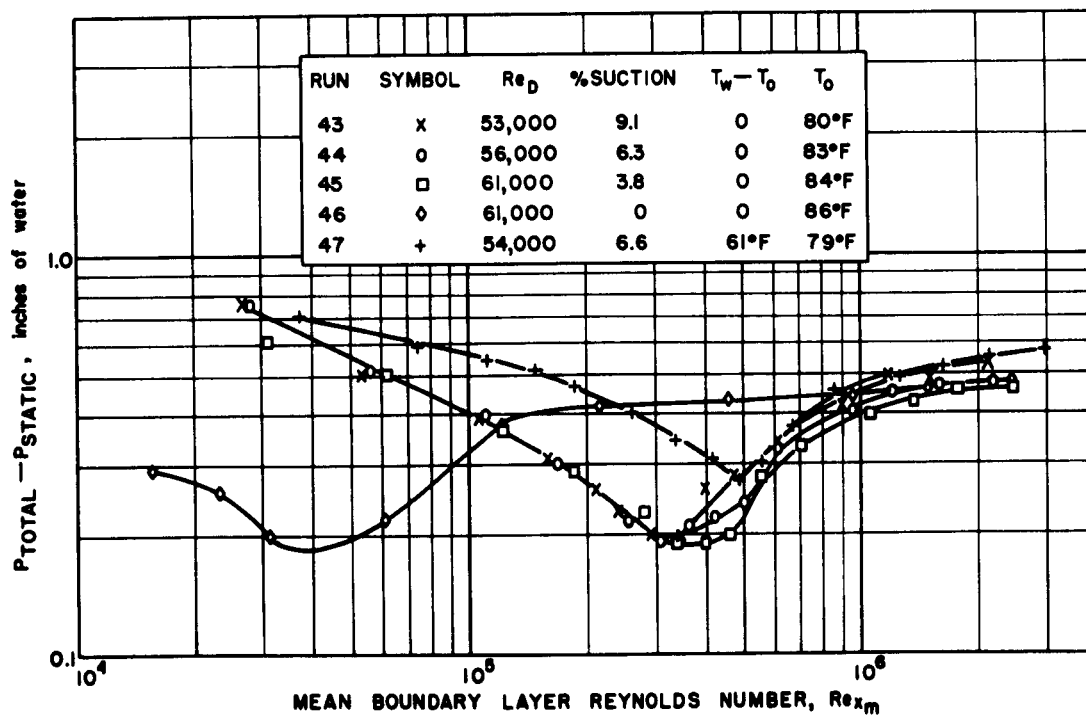

FIG. 18   THE EFFECT   OF   HEATING   ON   TRANSITION.   SAME   AS
FIG. 17,   EXCEPT   THAT   THE   MEAN   BOUNDARY   LAYER
REYNOLDS   NUMBER   IS   USED   IN   PLACE   OF   THE
FREE   STREAM   REYNOLDS   NUMBER.

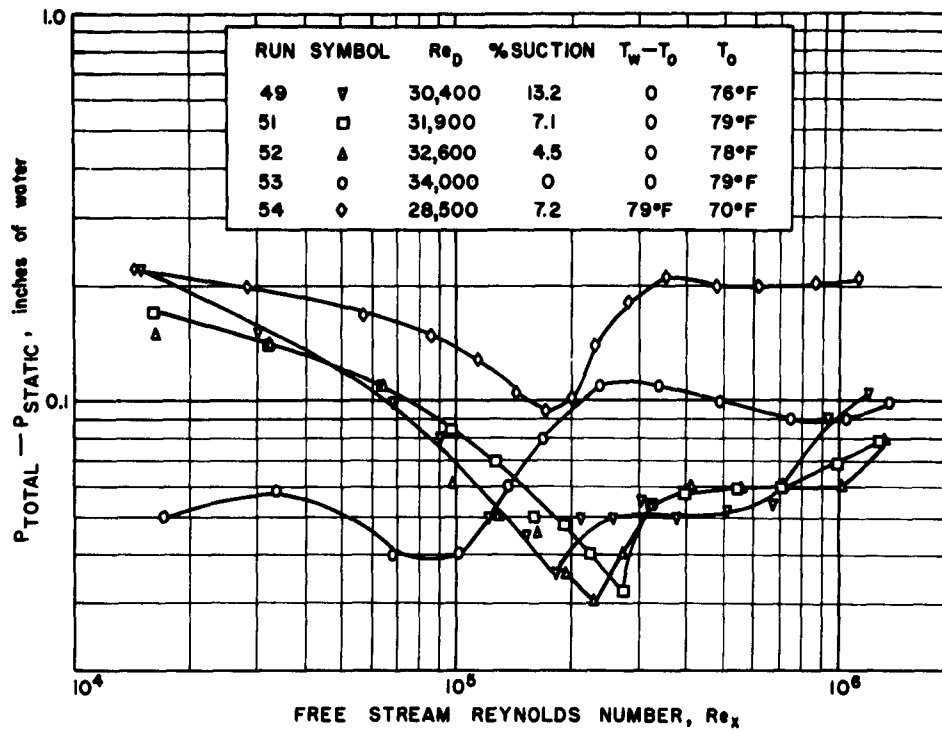| RUN	SYMBOL	Re_D	%SUCTION	T_w-T_o	T_o
49	▽	30,400	13.2	0	76°F
51	□	31,900	7.1	0	79°F
52	▲	32,600	4.5	0	78°F
53	○	34,000	0	0	79°F
54	◇	28,500	7.2	79°F	70°F

FIG. 19   THE EFFECT OF HEATING ON TRANSITION FOR A LOW
FLOW RATE WITH $Re_D \approx 30,000$.   THE EFFECT OF
BOUNDARY LAYER SUCTION RATE ON THE ADIABATIC
PERFORMANCE OF THE SYSTEM FOR THIS Re_D IS
ALSO SHOWN.

RUN	SYMBOL	Re_D	%SUCTION	T_w-T_o	T_o
49	▽	30,400	13.2	0	76°F
51	□	31,900	7.1	0	79°F
52	▲	32,600	4.5	0	78°F
53	○	34,000	0	0	79°F
54	◇	28,500	7.2	79°F	70°F

FIG. 20   THE EFFECT OF HEATING ON TRANSITION.   SAME AS
FIG. 19, EXCEPT THAT THE MEAN BOUNDARY LAYER
REYNOLDS NUMBER IS USED IN PLACE OF THE
FREE STREAM REYNOLDS NUMBER.

RUN	SYMBOL	Re_D	% SUCTION	$T_w - T_o$	T_o
60	o	70,500	5.3	0	75°F
61	□	74,100	3.2	0	78°F
62	▽	80,500	5.3	97°F	86°F

FREE STREAM REYNOLDS NUMBER, Re_x

FIG. 21   THE EFFECT OF HEATING ON TRANSITION.   CLEANING   THE
SYSTEM BEFORE THE RUNS WERE TAKEN HAS CAUSED
THE VALUE OF Re_x AT TRANSITION TO BE TWICE THE
VALUE SHOWN IN FIGS. 19 & 20.

RUN	SYMBOL	Re_D	% SUCTION	$T_w - T_o$	T_o
60	o	70,500	5.3	0	75°F
61	□	74,100	3.2	0	78°F
62	▽	80,500	5.3	97°F	86°F

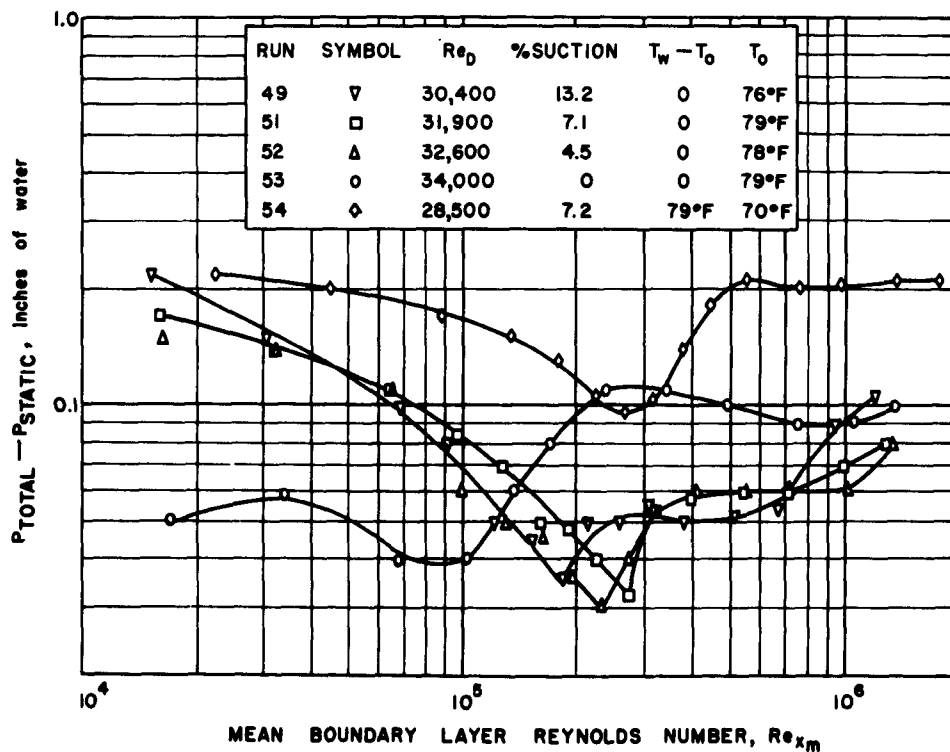MEAN BOUNDARY LAYER REYNOLDS NUMBER, Re_{x_m}

FIG. 22   THE EFFECT OF HEATING ON TRANSITION.   SAME AS
FIG. 21, EXCEPT THAT THE MEAN BOUNDARY LAYER
REYNOLDS NUMBER IS USED IN PLACE OF THE FREE
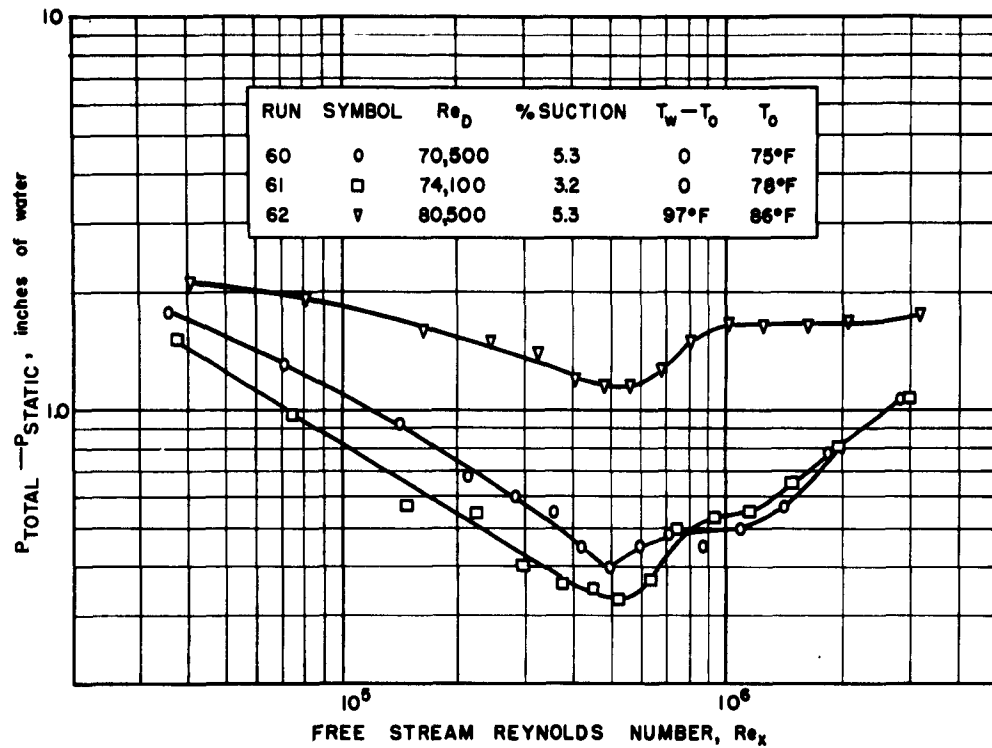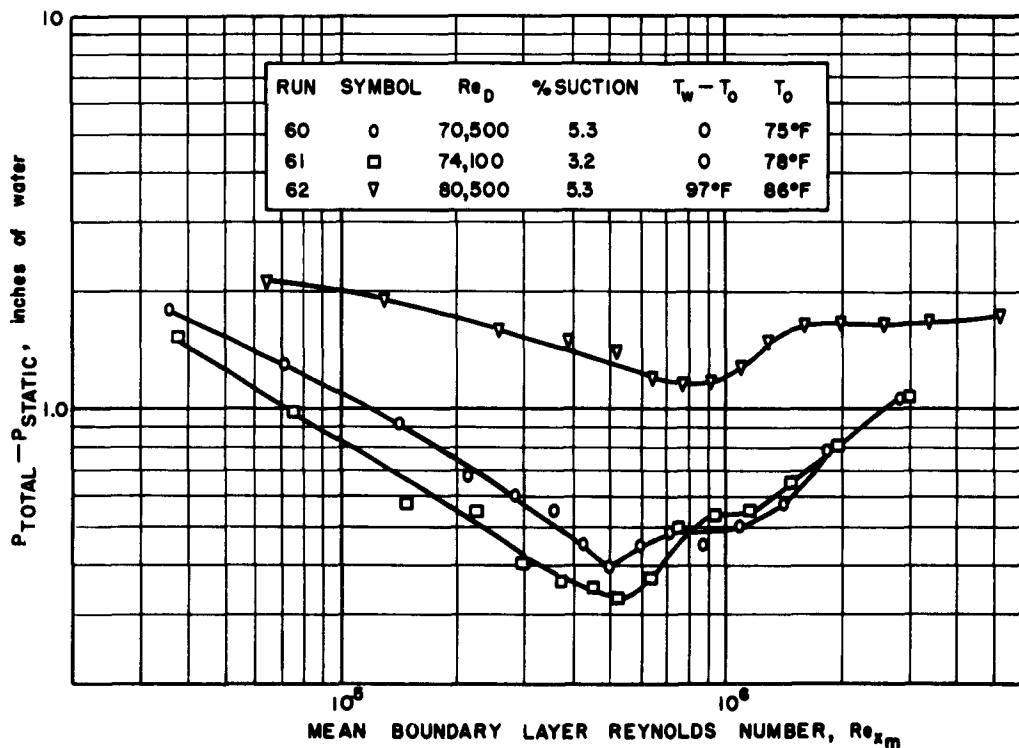STREAM REYNOLDS NUMBER.

RUN	SYMBOL	Re_D	%SUCTION	$T_w - T_o$	T_o
64	△	62,300	4.2	0	73°F
65	□	64,500	2.4	0	75°F
66	○	63,800	5.9	0	75°F
67	◇	61,100	3.8	98°F	72°F

FREE STREAM REYNOLDS NUMBER, Re_x

FIG. 23   THE EFFECT OF HEATING ON TRANSITION.   A VERY
THOROUGH CLEANING HAS INCREASED THE ADIABATIC
Re_x AT TRANSITION TO 850,000.

RUN	SYMBOL	Re_D	%SUCTION	$T_w - T_o$	T_o
64	△	62,300	4.2	0	73°F
65	□	64,500	2.4	0	75°F
66	○	63,800	5.9	0	75°F
67	◇	61,100	3.8	98°F	72°F

MEAN BOUNDARY LAYER REYNOLDS NUMBER, Re_{x_m}

FIG. 24   THE EFFECT OF HEATING ON TRANSITION.   SAME AS
FIG. 23, EXCEPT THAT THE MEAN BOUNDARY LAYER
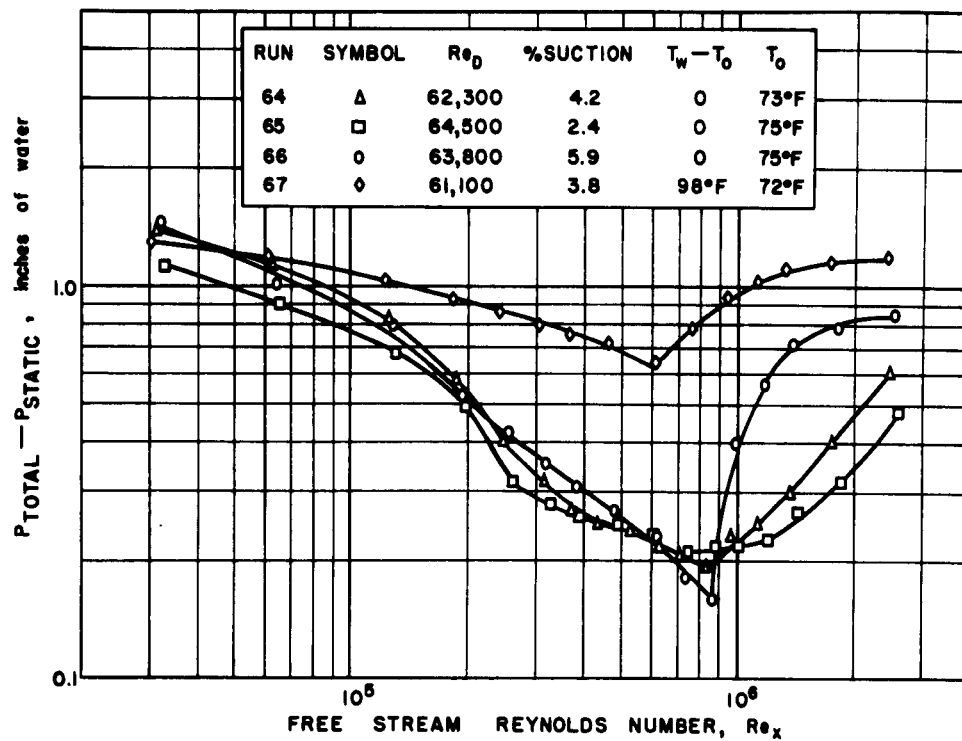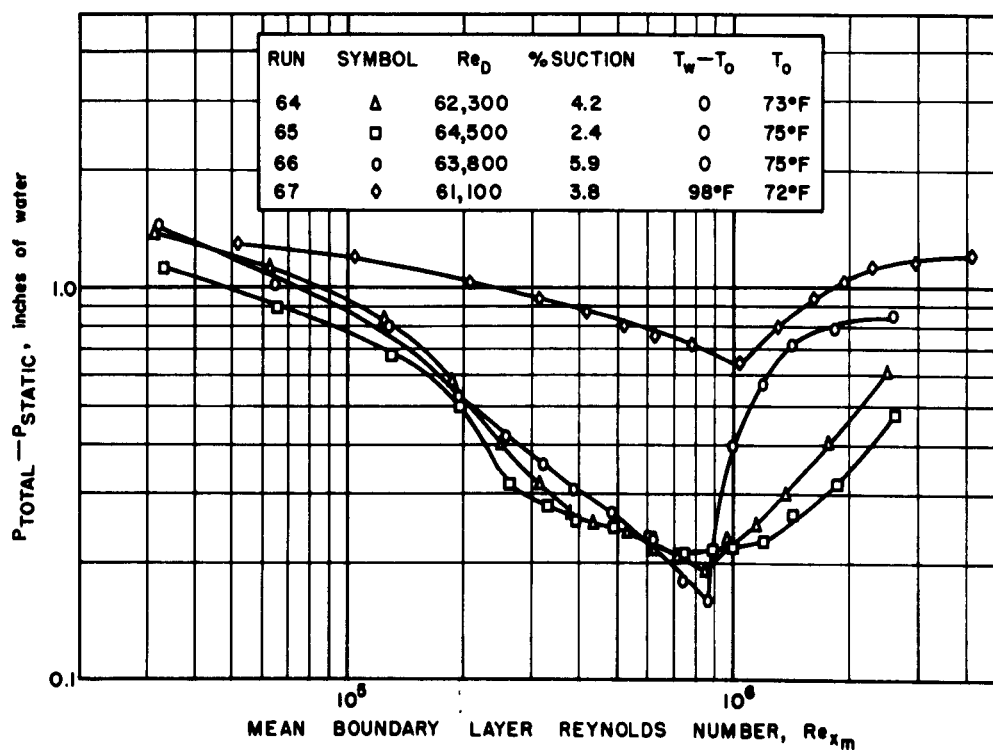REYNOLDS NUMBER IS USED IN PLACE OF THE
FREE STREAM REYNOLDS NUMBER.

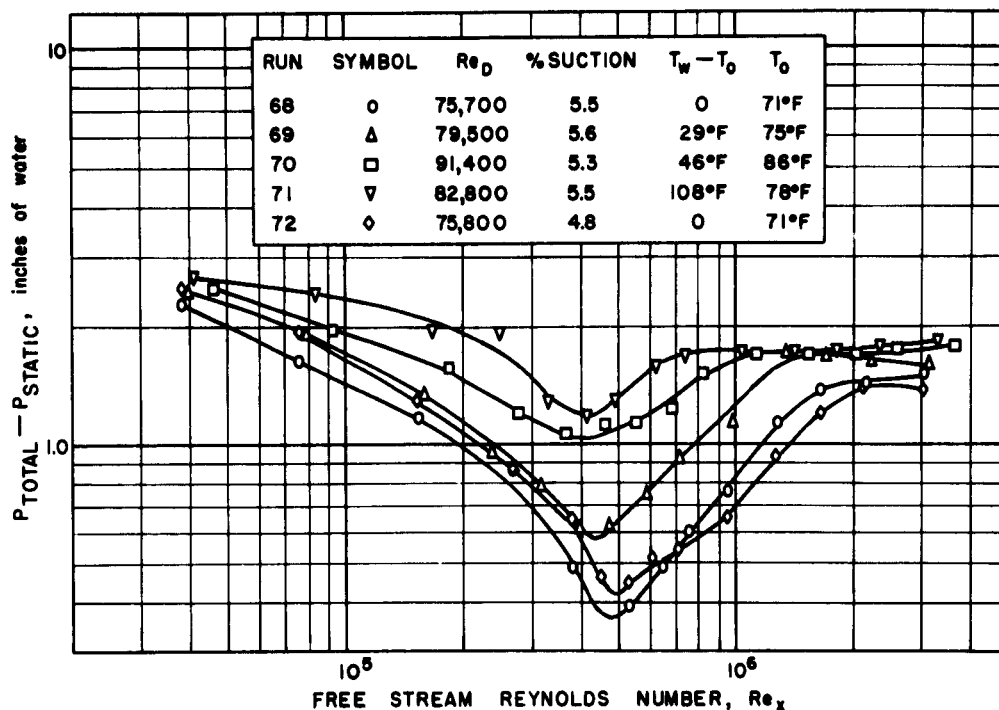| RUN	SYMBOL	Re$_D$	% SUCTION	T$_w$ — T$_o$	T$_o$
68	o	75,700	5.5	0	71°F
69	Δ	79,500	5.6	29°F	75°F
70	□	91,400	5.3	46°F	86°F
71	▽	82,800	5.5	108°F	78°F
72	◇	75,800	4.8	0	71°F

FIG. 25 THE EFFECT OF HEATING ON TRANSITION. INCREASING THE TEMPERATURE DIFFERENCE BETWEEN THE WALL AND FREE STREAM HAS CAUSED A CORRESPONDING INCREASE IN THE UPWARD DISPLACEMENT OF THE CURVES.

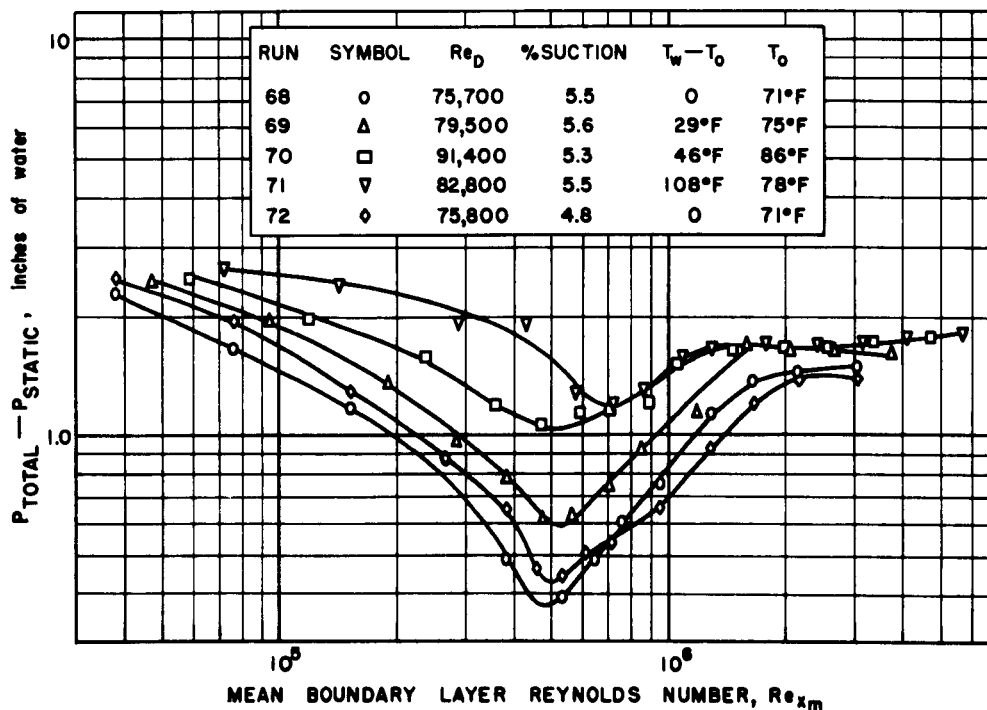| RUN	SYMBOL	Re$_D$	% SUCTION	T$_w$ — T$_o$	T$_o$
68	o	75,700	5.5	0	71°F
69	Δ	79,500	5.6	29°F	75°F
70	□	91,400	5.3	46°F	86°F
71	▽	82,800	5.5	108°F	78°F
72	◇	75,800	4.8	0	71°F

FIG. 26 THE EFFECT OF HEATING ON TRANSITION. SAME AS FIG. 25, EXCEPT THAT THE MEAN BOUNDARY LAYER REYNOLDS NUMBER IS USED IN PLACE OF THE FREE STREAM REYNOLDS NUMBER. INCREASING THE TEMPERATURE DIFFERENCE HAS CAUSED AN INCREASE IN THE MEAN BOUNDARY LAYER LENGTH REYNOLDS NUMBER OF TRANSITION.
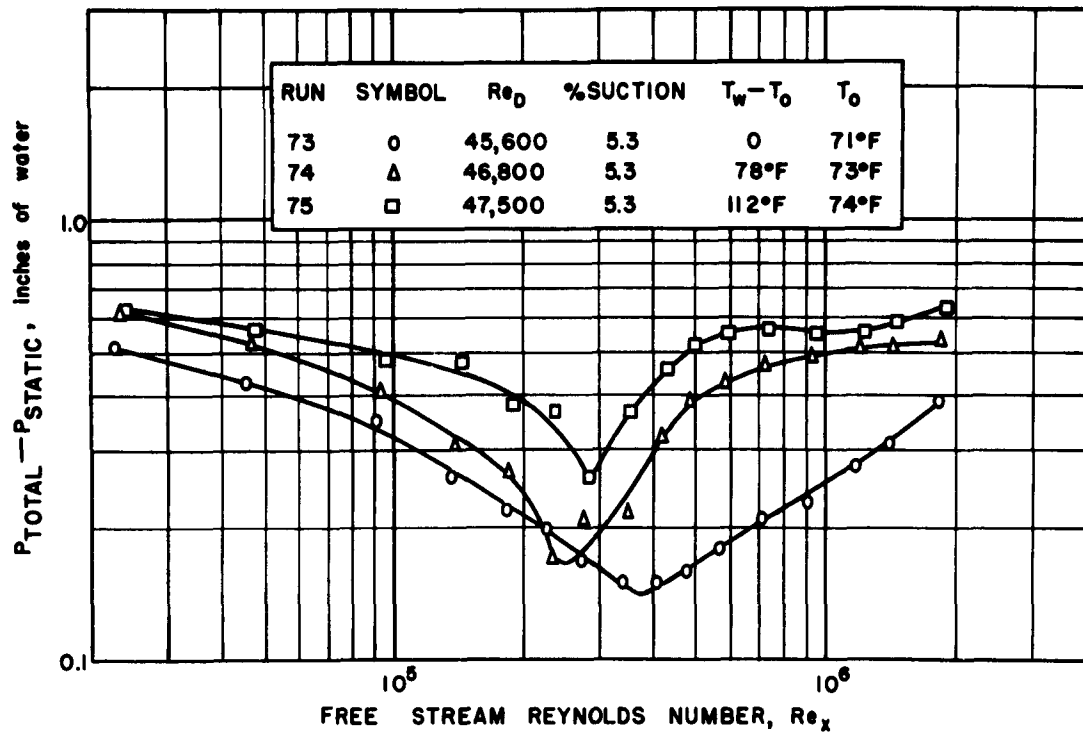
RUN	SYMBOL	Re_D	%SUCTION	T_w-T_o	T_o
73	o	45,600	5.3	0	71°F
74	Δ	46,800	5.3	78°F	73°F
75	□	47,500	5.3	112°F	74°F

FIG. 27   THE EFFECT OF HEATING ON TRANSITION.   THESE   CURVES, TAKEN AT A LOWER FLOW RATE, EXHIBIT THE SAME CHARACTERISTICS   SHOWN   IN   FIG. 25.

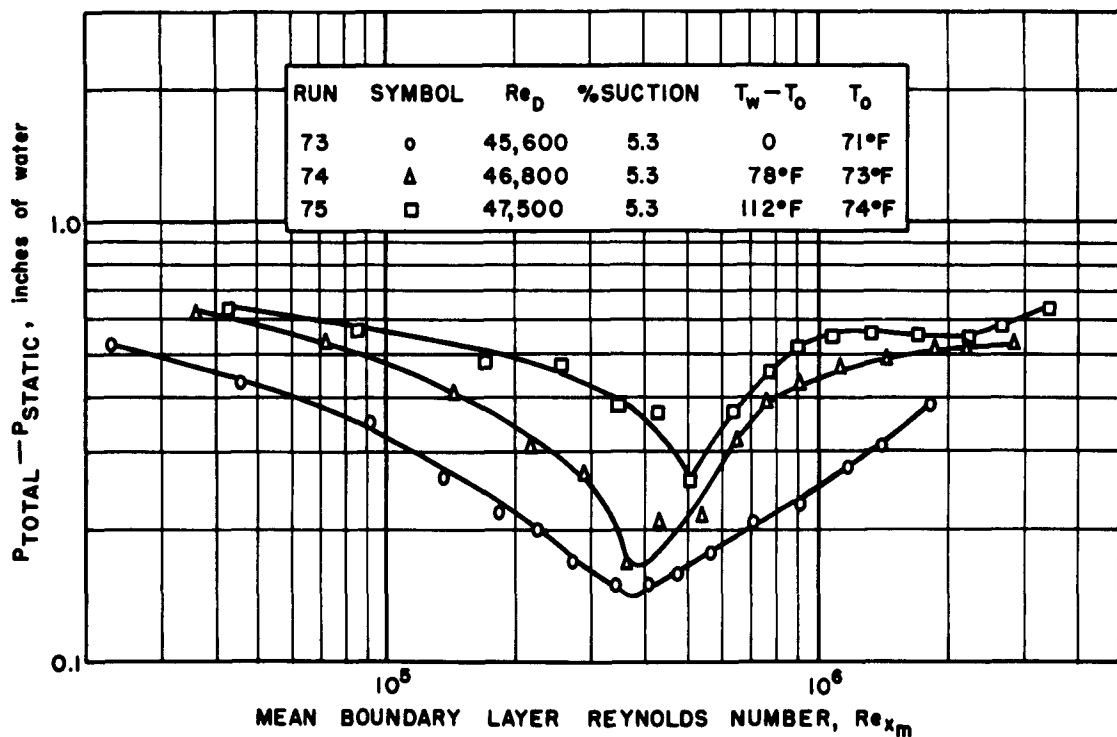| RUN	SYMBOL	Re_D	%SUCTION	T_w-T_o	T_o
73	o	45,600	5.3	0	71°F
74	Δ	46,800	5.3	78°F	73°F
75	□	47,500	5.3	112°F	74°F

FIG. 28   THE EFFECT OF HEATING ON TRANSITION.   SAME   AS FIG. 27, EXCEPT THAT THE MEAN BOUNDARY LAYER REYNOLDS IS USED IN PLACE OF THE FREE STREAM REYNOLDS NUMBER.
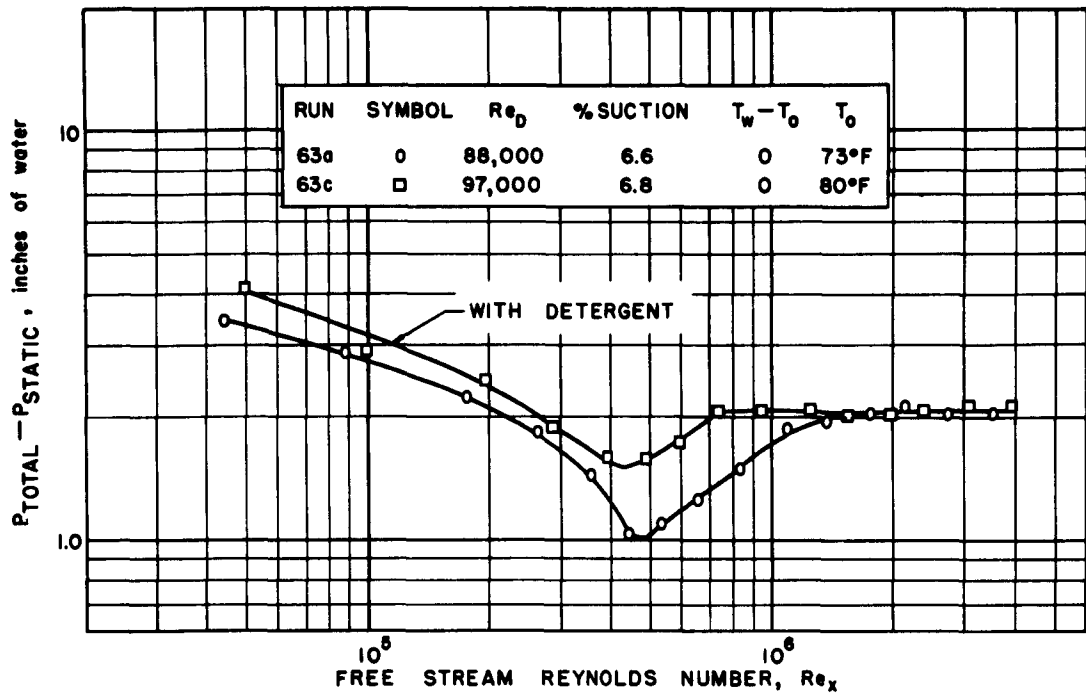
RUN	SYMBOL	Re_D	% SUCTION	$T_W - T_O$	T_O
63a	O	88,000	6.6	0	73°F
63c	□	97,000	6.8	0	80°F

WITH DETERGENT

FIG. 29 ADIABATIC CURVES SHOWING THAT THE ADDITION OF DETERGENT TO THE SYSTEM DID NOT INFLUENCE TRANSITION.

DATA OF KLINE AND SHAPIRO[6]
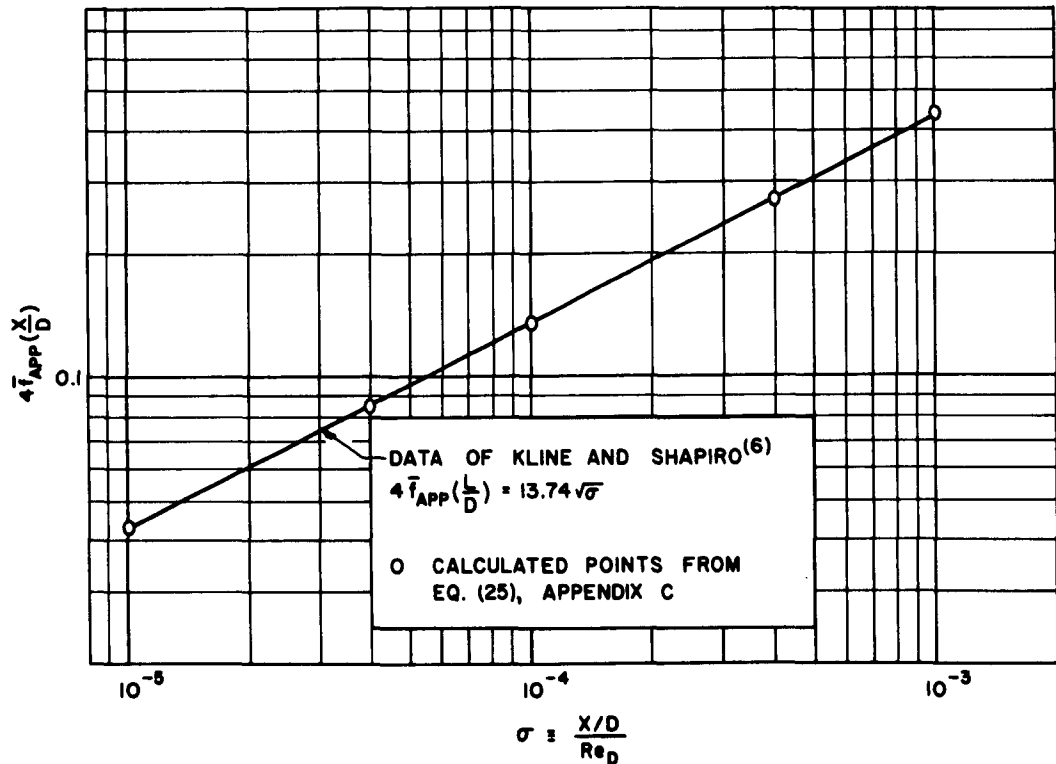
$$4\bar{f}_{APP}\left(\frac{L}{D}\right) = 13.74\sqrt{\sigma}$$

O CALCULATED POINTS FROM EQ. (25), APPENDIX C

$$\sigma = \frac{X/D}{Re_D}$$

FIG. 30 COMPARISON OF THE RESULTS OF THEORETICAL FRICTION FACTOR COMPUTATIONS FOR THE LAMINAR ENTRY OF A TUBE WITH THE DATA OF KLINE AND SHAPIRO[6].
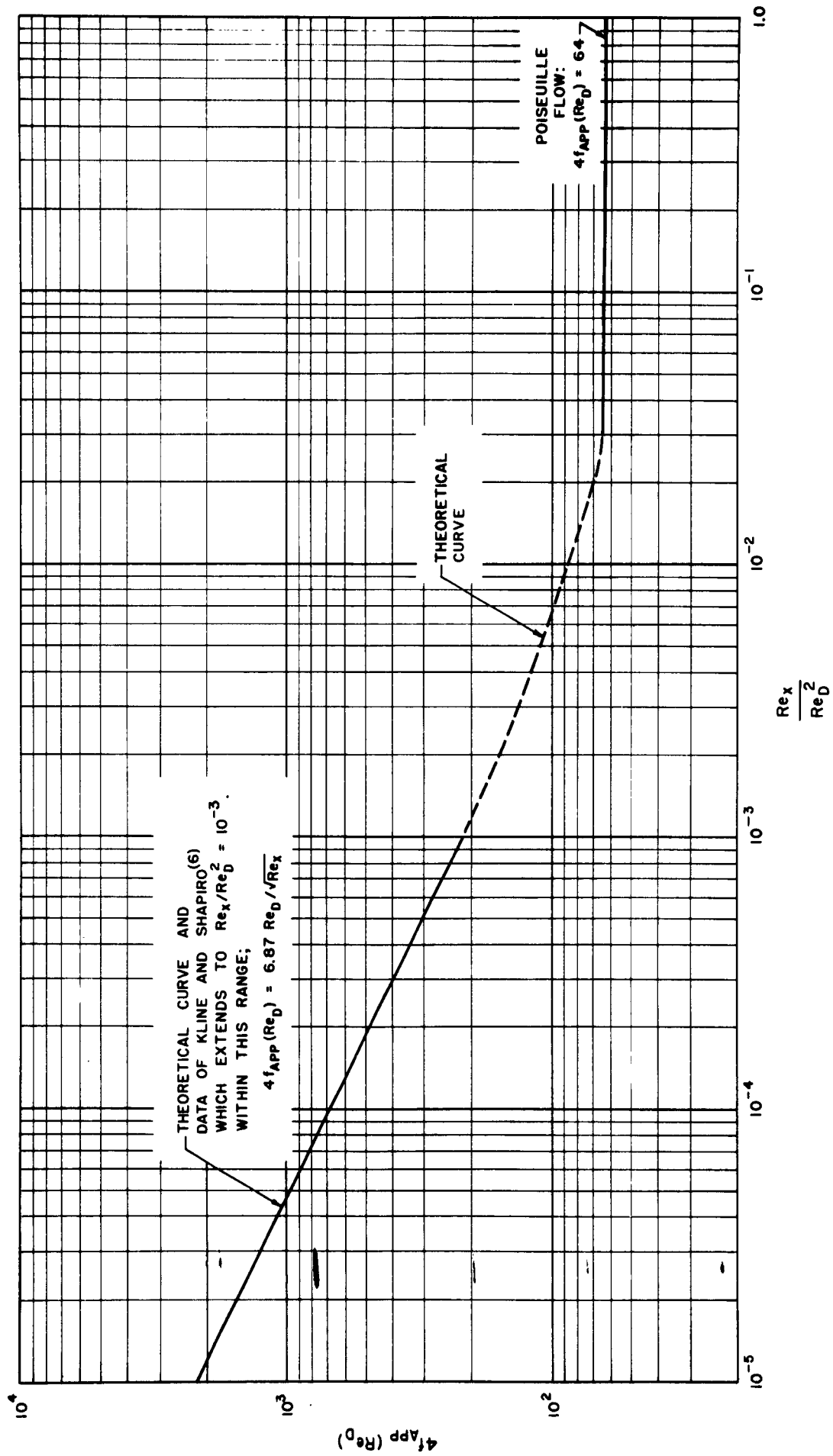
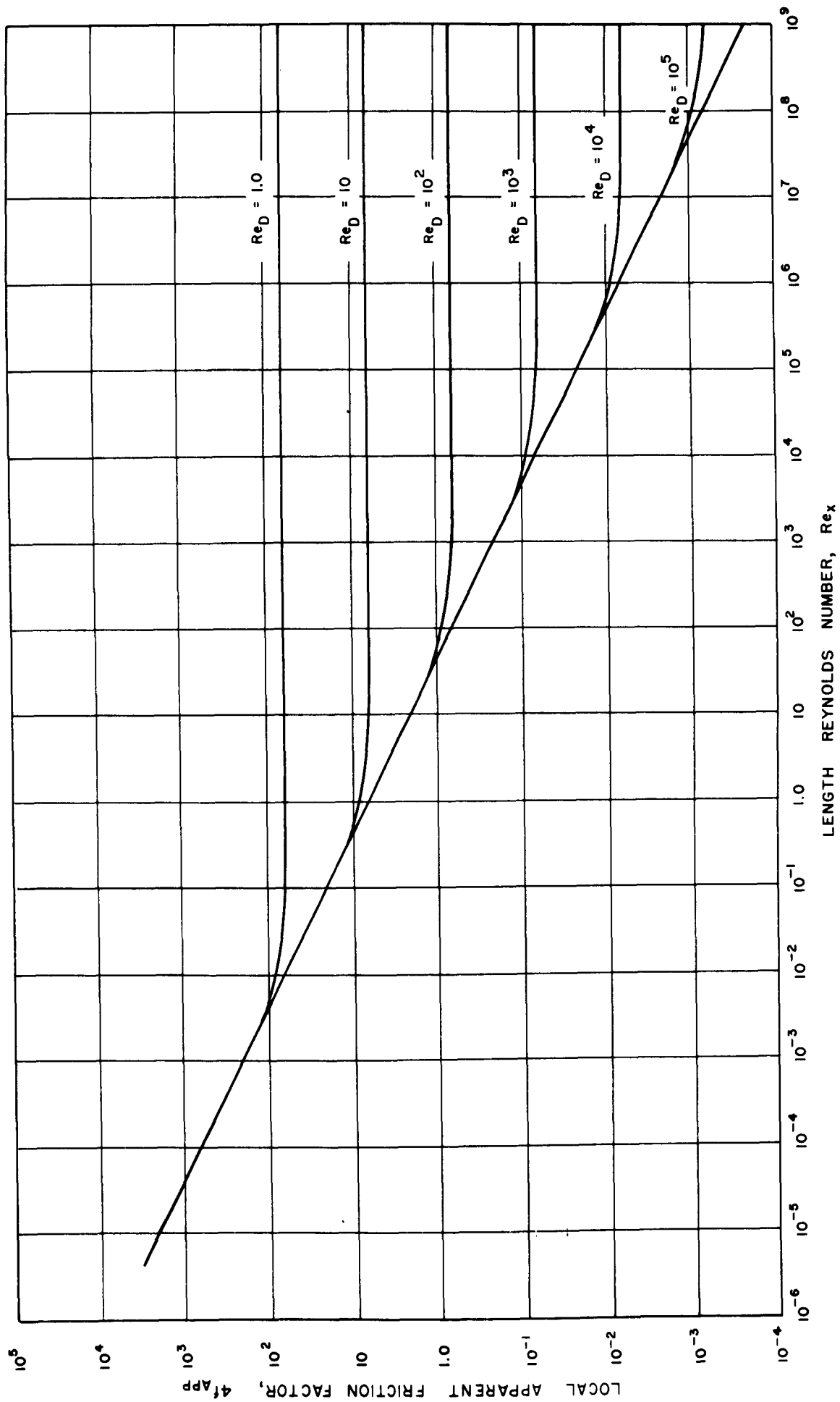FIG. 32 GENERALIZED CURVE OF LOCAL APPARENT FRICTION FACTOR IN A LAMINAR TUBE ENTRY

FIG. 33   FAMILY   OF   CURVES   OF   LOCAL   APPARENT   FRICTION   FACTOR   vs. Re_x IN   A   LAMINAR
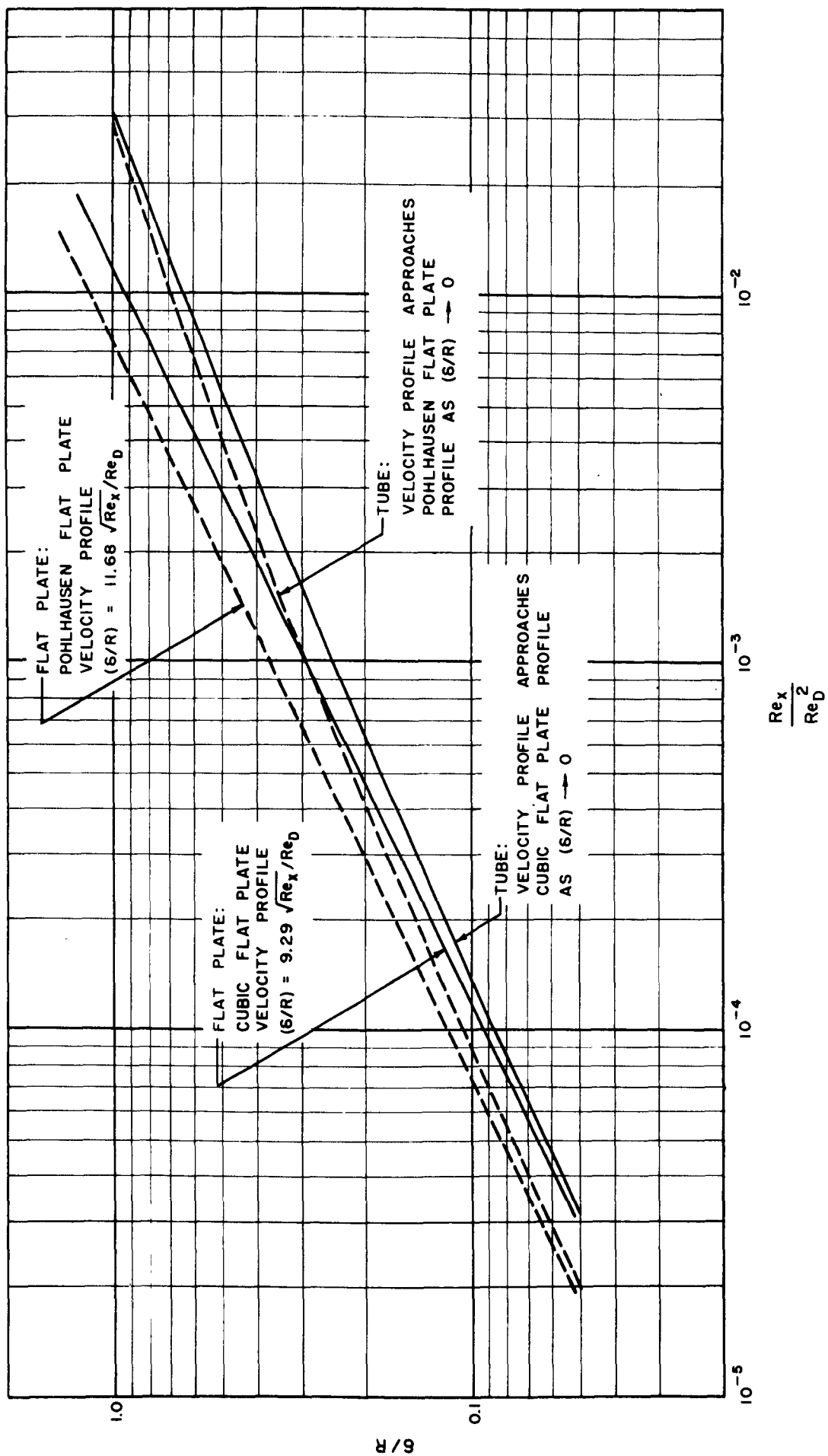TUBE   ENTRY,   FOR   SEVERAL   VALUES   OF Re_D

FIG. 34   BOUNDARY LAYER GROWTH IN A LAMINAR TUBE ENTRY AS COMPARED WITH THE GROWTH ON A FLAT PLATE